

1 **Protein Kinase Structure and Dynamics: Role of the α C- β 4 Loop**

2

3

4 Jian Wu¹, Nisha A. Jonniya¹, Sophia P. Hirikis², Cristina Olivieri³, Gianluigi Veglia^{3,4}, Alexandr P.

5 Kornev¹, Susan S. Taylor^{1, 2*}

6

7 ¹ Department of Pharmacology, University of California, San Diego, La Jolla, CA 92037-

8 0654, USA.

9 ² Department of Chemistry and Biochemistry, University of California, San Diego, La

10 Jolla, CA 92037-0654, USA.

11 ³ Department of Biochemistry, Molecular Biology, and Biophysics, University of

12 Minnesota, MN 55455, USA.

13 ⁴ Department of Chemistry, University of Minnesota, MN 55455, USA.

14

15

16 * Corresponding author:

17 Susan S. Taylor

18 Department of Pharmacology and Department of Chemistry and Biochemistry

19 University of California, San Diego, La Jolla, CA 92037-0654, USA

20 Email: staylor@ucsd.edu

21

22 **Abstract**

23 Although the α C- β 4 loop is a stable feature of all protein kinases, the importance of this motif
24 as a conserved element of secondary structure, as well as its links to the hydrophobic
25 architecture of the kinase core, has been underappreciated. We first review the motif and then
26 describe how it is linked to the hydrophobic spine architecture of the kinase core, which we first
27 discovered using a computational tool, Local Spatial Pattern (LSP) alignment. Based on NMR
28 predictions that a mutation in this motif abolishes the synergistic high-affinity binding of ATP and
29 a pseudo substrate inhibitor, we used LSP to interrogate the F100A mutant. This comparison
30 highlights the importance of the α C- β 4 loop and key residues at the interface between the N-
31 and C-lobes. In addition, we delved more deeply into the structure of the apo C-subunit, which
32 lacks ATP. While apo C-subunit showed no significant changes in backbone dynamics of the
33 α C- β 4 loop, we found significant differences in the side chain dynamics of K105. The LSP
34 analysis suggests disruption of communication between the N- and C-lobes in the F100A
35 mutant, which would be consistent with the structural changes predicted by the NMR
36 spectroscopy.

37

38

39 **Introduction.** Although the protein kinases, like the GTPases, have evolved to be highly
40 regulated molecular switches, they transfer the γ -phosphate of adenosine triphosphate (ATP) to
41 a protein substrate instead of to water. Understanding how mature and fully active protein
42 kinases couple ATP binding to peptide/protein binding is especially challenging as it involves
43 many sites that lie distal to the active site. This process of phosphorylating a heterologous
44 protein substrate should be clearly distinguished from *cis*-autophosphorylation of the kinase
45 core, which is usually a key initial step in the assembly of most active kinases. *Cis*-
46 autophosphorylation of a protein kinase core is distinct and different from transferring the
47 phosphate to a heterologous protein. In cells a fully active kinase transfers the γ -phosphate of
48 ATP to a heterologous protein substrate that is typically tethered to a distal site that lies far from
49 the site of phosphoryl transfer. To ask how a mature and fully active protein kinase couples ATP
50 binding to peptide/protein binding we use the catalytic (C) subunit of cAMP-dependent protein
51 kinase (PKA) as a model system. PKA activity is regulated by inhibitory regulatory (R) subunits
52 and by heat-stable protein kinase inhibitors (PKIs). In addition, we have extensive NMR data
53 and computational analyses of PKA that complement crystal structures and provide essential
54 windows into dynamics.

55 The conserved motifs that define the kinase core were first recognized when Dayhoff
56 aligned the cloned sequence of Src with the manually sequenced C-subunit of PKA in 1982 (1).
57 By manually aligning a handful of protein kinases, Hanks, et al, subsequently showed that these
58 motifs, which were scattered throughout the kinase core, were conserved in all protein kinases
59 (2). When the first protein kinase structure was solved in 1991, these conserved sequence
60 motifs became structural entities that correlated with β strands, α helices, and loops of the
61 folded protein (3). That first structure, which was actually a binary complex of the PKA C-subunit
62 and an inhibitory peptide (IP20) from PKI, also provided a detailed description of how the IP20
63 peptide was docked onto the kinase core (4). Subsequent structures of a ternary complex with
64 ATP and IP20, solved in 1993, showed how the conserved motifs correlated with ATP and
65 peptide binding and engaged the entire kinase core (5, 6). Although Johnson provided a more
66 detailed description of these motifs (7), several essential points were not yet understood. Only
67 later, using computational tools, did we come to appreciate how the conserved and non-linear
68 hydrophobic core architecture was assembled and how hydrophobicity correlated with allosteric
69 regulation of the kinase core (8-10). In addition, we did not initially appreciate the importance of
70 the α C- β 4 loop. Like helices and strands, the α C- β 4 loop is also a well-defined element of
71 secondary structure (11, 12), and this loop in the N-terminal lobe (N-Lobe) of the kinase core is
72 essential for mediating the synergistic high-affinity binding of ATP and IP20.

73 Unlike other protein kinases such as PKC and the Leucine-rich repeat kinase 2 (LRRK2)
74 that are flanked by other domains that regulate activation and subcellular localization (13-15),
75 the PKA C-subunit represents a kinase domain that is flanked by relatively short N- and C-
76 terminal tails (16). In cells the C-subunit is then assembled as an inactive holoenzyme with
77 functionally non-redundant cAMP binding regulatory (RI α , RI β , RII α , and RII β) subunits allowing
78 the activity of the kinase domain to be unleashed rapidly and reversibly by allosteric binding of
79 cAMP to the cyclic-nucleotide binding domains (CNB) of the R-subunits (17). In addition, the
80 PKA C-subunit can be regulated by PKI. The R-subunits and PKI all share an inhibitor site that
81 docks to the active site cleft of the C-subunit; however, PKI and RI α /RI β are unusual in that they
82 are pseudo substrates where high-affinity binding is synergistically coupled to the high-affinity
83 binding of ATP (~60nM). Even though the structure of the PKA C-subunit was solved over 30
84 years ago, we still are elucidating the mechanistic details of how the highly dynamic features of
85 the kinase core are regulated by a set of well-defined motifs and, in particular, how the high-
86 affinity binding of ATP and IP20 are coupled. Disease mutations are also providing key
87 mechanistic insights into how the synergistic binding of ATP and PKI can be uncoupled. Using
88 the PKA C-subunit as a prototype, we focus here, in particular, on the conserved hydrophobic
89 residues/motifs that define the core protein kinase architecture, which contributes so
90 significantly to entropy-driven allostery (18). We then describe how the α C- β 4 loop is anchored
91 to the hydrophobic core architecture. Finally, we explore how a single mutation, F100A in the
92 α C- β 4 loop, uncouples the synergistic binding of ATP and PKI using a computational approach
93 that first identified the hydrophobic spines (8, 9).

94
95 **Discovering the hydrophobic core architecture of protein kinases.** While we elucidated
96 conserved motifs in the kinase core early on (1, 2, 7) and identified, using affinity labeling,
97 specific residues that we hypothesized were associated with ATP binding (19, 20), we did not
98 have a thorough understanding of the bilobal kinase fold until the first protein kinase structure
99 was solved. This first structure defined the N-Lobe and the C-Lobe and validated the active site
100 localization of the regulatory triad that was identified by affinity labeling and cross-linking. This
101 triad consists of two residues in the N-Lobe - K72 in β 3 and E91 in the α C-Helix and one in the
102 DFG motif in the C-Lobe - D184 (3). The subsequent structures in 1993 (5, 6) showed how ATP
103 was held into the active site cleft between the two lobes. Together, these structures validated
104 the affinity labeling experiments where the three motifs containing the regulatory triad residues
105 converged on the ATP phosphates and Mg²⁺ ions at the active site cleft. This structure of a fully

106 closed conformation also defined a novel ATP binding motif where the adenine ring of ATP was
107 buried under a Glycine-rich Loop (G-loop) in a pocket at the base of the cleft (5, 6). From these
108 early structures we gain an appreciation for what is now called the “Activation Loop”. The
109 Activation loop is typically assembled by a key phosphorylation site (21, 22), and this loop is
110 very stable in the PKA C-subunit because T197 is constitutively phosphorylated in the purified
111 C-subunit. At that time, however, we did not appreciate the highly dynamic features that
112 regulate kinase activity, including the Activation loop, nor did we appreciate the role of
113 hydrophobicity in driving dynamics. This would require both computational tools that were not
114 yet sufficiently robust as well as nuclear magnetic resonance (NMR) spectroscopy. In addition,
115 we would need structures of other kinases where the Activation loop is typically disordered (21,
116 22).

117 The importance of hydrophobic residues and the concept of non-contiguous but spatially
118 conserved hydrophobic motifs, some highly conserved and others just conserved as
119 hydrophobic residues, did not become obvious until we investigated structural differences with a
120 computational approach called Local Spatial Pattern (LSP) alignment. With LSP alignment we
121 first identified spatially conserved residues that revealed a conserved hydrophobic “spine”
122 architecture that was associated with active kinases but broken in inactive kinases (8). The
123 terminology of “spines” is related to the fluidity of these residues in contrast to hydrophilic
124 residues and ion pairs that are locked into a more rigid conformation by hydrogen bonds or
125 electrostatic bonds. The Regulatory Spine (R-spine) residues were identified first and
126 correspond to four spatially conserved residues - two in the C-lobe and two in the N-lobe that
127 were aligned in every active kinase but broken in inactive kinases (8). The assembly of the R-
128 Spine defines the switch mechanism of every active kinase. It reveals how kinases have
129 evolved to be dynamic molecular switches, similar to the GTPases. In contrast to metabolic
130 enzymes, they have not evolved to be efficient catalysts. The highly regulated R-Spine along
131 with the Regulatory Triad (K72/E91/D184) remain as hallmark signature motifs of every active
132 kinase that is capable of trans-phosphorylation of a heterologous protein substrate.

133 A second motif, referred to as the Catalytic Spine (C-Spine), defines the extensive and
134 fundamental core hydrophobic architecture of every kinase domain (9). The C-spine includes
135 motifs in both the N-Lobe and the C-Lobe, which are connected by the hydrophobic capping of
136 the adenine ring of ATP. Capping of the adenine ring is accomplished by two highly conserved
137 residues (A70 in $\beta 3$ and V57 in $\beta 2$) in the N-Lobe while the other surface of the adenine ring is
138 capped by a C-Lobe residue, L173 in $\beta 7$, which is a conserved hydrophobic residue found in all
139 kinases. The dominant feature of the C-spine is the very unusual hydrophobic α F-Helix that

140 spans the C-lobe and is linked to all of the important elements of the C-Lobe (**Figure 1**). This
141 buried helix is unusual for several reasons. With a conserved glycine in the middle, it does not
142 have a strong helical propensity. In general, it is highly unusual to find a buried hydrophobic
143 helix in a globular domain; in many ways it is more like a trans membrane helix. The α F helix is
144 flanked by two charged residues. At the beginning of the α F Helix is the highly conserved D220
145 that couples the α F Helix to the catalytic machinery at the active site cleft (**Figure 2**).
146 Specifically, it hydrogen bonds to the backbone amides of Y164 and R165 in the Y/HRD motif
147 that precedes the catalytic loop. D220 is followed by another highly conserved residue, W222,
148 which faces the α H- α I loop, a tethering site on the bottom of the C-Lobe (23, 24). W222 also
149 shields the conserved ion pair between E208 at the end of the APE motif and R280 in the α H- α I
150 loop. At the other end of the α F Helix is E230 which in PKA recognizes the P-2 arginine in the
151 substrate peptide/protein. The remarkable features of the α F-Helix that allow it to be the central
152 organizing unit of the C-lobe, summarized in **Figure 1**, were clearly revealed in the LSP plots in
153 2008 (9). What was not fully appreciated in these first analyses, however, was the role of the
154 α E-Helix in the C-Lobe and another highly conserved motif in the N-Lobe, the α C- β 4 loop.

155
156 **The α C- β 4 Loop.** The two spine residues in the N-Lobe, which lie at the end of the α C Helix
157 (RS3) and the beginning of β 4 (RS4), stabilize a very important element of secondary structure
158 that is conserved in every protein kinase - the α C- β 4 loop (residues 99-106) (**Figure 3**). The two
159 R-spine residues are brought together by a strategic β -turn motif (residues 100-103) where the
160 carbonyl of F100 is hydrogen bonded to the backbone amide of L103 (11). The other carbonyls
161 and amides of this turn, as well as those of the other residues in this motif, are filled by ordered
162 water molecules (**Figure 3B**). Structured water molecules highlight that this surface of the α C-
163 β 4 loop is exposed to solvent, while the other buried surface of the α C- β 4 motif is very
164 hydrophobic and anchored to the hydrophobic R-Spine and Shell residues (25). Only one
165 residue in the α C- β 4 motif, V104, directly touches ATP through one of its methyl side chains
166 that is anchored to the adenine ring.

167 Although highly conserved and very stable, this β -turn is not traditionally recognized as a
168 stable element of secondary structure (12). The two N-lobe spine residues (RS3 and RS4)
169 anchor the α C- β 4 motif to the R-Spine residues in the C-Lobe (**Figure 3B**) while the tip of the
170 loop is very hydrophobic (**Figure 3A**). The critical features at the tip of the β -turn typically
171 include a proline. Even though the backbone amides and carbonyls of the β -turn are solvent
172 exposed, one can see in PKA that the hydrophobic side chain residues at the tip of the loop,

173 F100-P101-F102-L103, are buried in a hydrophobic pocket comprised primarily of residues in
174 the α E-Helix. The strategic importance of stabilizing the backbone of this α C- β 4 loop is
175 highlighted by Y156 in the α E helix, which hydrogen bonds to the backbone amide of N99.
176 Although this residue (N99) is not conserved, its functional importance has been highlighted by
177 BRAf where replacement of this residue (R509) with histidine breaks the BRAf dimer interface
178 that is essential for BRAf activation (26, 27). The importance of this residue was also explored in
179 depth for the EGF receptor where this site is a hot spot for oncogenic mutations (28, 29).
180 Although the residue at the N99 position differs in every kinase, its spatial organization as well
181 as the hydrogen bonding of its backbone to the α E helix is conserved, and its strategic function
182 may also be conserved.

183 The first 600 picosecond Molecular Dynamics (MD) simulations of the PKA C-subunit,
184 published in 1999, not only demonstrated that the N-Lobe and the C-Lobe function as
185 independent rigid bodies but also showed that the α C- β 4 loop (residues 99-106) is the only
186 piece of the N-lobe that remains anchored to the C-lobe whether the kinase is in an open or
187 closed conformation (30) (**Figure 4**). We now know from many kinase structures that positioning
188 and organizing the N-lobe for catalysis is complex and highly regulated. The analysis of LRRK2
189 supports the prediction that the N- and C-lobes of the kinase core function as independent rigid
190 bodies (31, 32). It also indicates that the α C- β 4 loop remains as one of the most stable
191 elements of the kinase core whether LRRK2 is in an active or an inactive conformation (**Figure**
192 **4**). The α C- β 4 loop is also stably anchored to the α E helix in the active and inactive Src as well
193 as in the active and inactive BRAF (**Figure 4**). Indeed, the α C- β 4 loop is conserved as a stable
194 element of secondary structure in every protein kinase as it anchors to the α E Helix.

195

196 **The α E Helix.** Although the dynamic α C Helix, as well as the stable α F Helix described above
197 (**Figure 1**), have been long recognized as conserved elements of the kinase core, less attention
198 has been given to the α E Helix. A defining feature of the α E Helix, mentioned above, is Y156.
199 This conserved tyrosine, which can also be a histidine or phenylalanine in other kinases, is
200 anchored to the backbone amide of N99 in the α C- β 4 loop. The importance of this residue is
201 highlighted in BRAF, as discussed previously. Two residues down from Y156 is H158 which in
202 PKA is firmly anchored to the conserved D220 in the α F Helix. H158 is one of three dually
203 protonated histidines in the C-subunit (33, 34). In the fully active C-subunit that is
204 phosphorylated on its Activation loop the side chain of His158 anchors the backbone amides of
205 the HRD residues (R165 and D166) in the Catalytic loop. In contrast to the Activation loop

206 (residues 184-pT197), which is dynamically assembled, the backbone of the catalytic machinery
207 in the C-Lobe (residues 162-182) is very stable. As seen in **Figure 2**, this interaction as well as
208 the hydrophobic anchoring of the catalytic loop to the α E and α F Helices makes the backbone of
209 the catalytic loop very stable. H158 is conserved as a histidine or phenylalanine in most
210 kinases and in the EGF receptor and in other tyrosine kinases this region is a hot spot for
211 oncogenic mutations (15).

212 I150 in the α E Helix is also a key residue. The importance of I150 as a critical player in
213 the hydrophobic core architecture was first highlighted by NMR (10). As seen in **Figure 2**, I150
214 is important for many reasons. It is anchored to L167 and P169 in the Catalytic loop and to L172
215 in β 7, which connects the adenine capping residue, L173, to the hydrophobic core. On the other
216 side of L173, both I174 and I180 in β 8 anchor the adenine capping residue to the α E Helix. In
217 contrast to the Activation Segment and the R-spine, which are dynamically assembled as part of
218 activation, the backbone residues of the catalytic machinery are always very stably anchored to
219 the hydrophobic core architecture. The two R-Spine residues in the C-Lobe, RS1 in the HRD
220 motif and RS2 in the DFG motif, are all highlighted in **Figure 2** where we can appreciate that the
221 catalytic machinery is anchored to the R-Spine, similar to the hydrophobic surface of the α C- β 4
222 loop.

223
224 **Synergistic high affinity binding of ATP and pseudo-substrate inhibitors.** A highly unusual
225 allosteric feature of PKA that is perhaps unique to PKA is its heat-stable protein kinase inhibitor
226 (PKI). PKI was first identified as a high-affinity inhibitor of the PKA C-subunit in 1971 shortly
227 after the C-subunit was discovered (35). It is a classic Intrinsically Disordered Protein (IDP), a
228 prediction that was fully validated recently by NMR of full-length PKI (36). Once it was
229 sequenced (37), PKI was shown to be a pseudosubstrate, a feature that is shared by the type I
230 Regulatory (R) Subunits of PKA, RI α and RI β . While the inhibitory properties of PKI were
231 localized to the N-terminus (residues 5-24) (38, 39), the unusual synergistic high-affinity binding
232 of ATP and PKI was characterized in detail by the peptide studies of Whitehouse and Walsh
233 (40). They confirmed that having a pseudo-substrate where the P-site in PKI is an alanine, is
234 essential for high affinity binding while the arginines that precede the P-site, as well as the P+1
235 hydrophobic residue, are also important for binding of both substrates and pseudosubstrates.
236 To achieve high-affinity binding, however, hydrophobic residues that preceded the inhibitor site
237 were required. Based on their peptide studies and subsequent biophysical studies, Walsh and
238 his colleagues predicted that this hydrophobic motif was an amphipathic helix (41-43).
239 Localization of the inhibitory region to the N-terminus of PKI and the rigorous characterization of

240 the inhibitor peptide (IP20, residues 5-24) enabled crystallization of that first PKA structure
241 bound to IP20 (3). A second paper (4), which completely validated the peptide predictions,
242 showed precisely how IP20 bound with high affinity through basic residues near the active site
243 and a distal amphipathic helix (**Figure 5**). Showing how both charged and hydrophobic residues
244 contribute to peptide binding at sites that are distal to the phosphoryl transfer site did not explain,
245 however, how the synergistic high-affinity binding of ATP and IP20 was achieved. The R1 α
246 subunit is also a pseudosubstrate and displays the same synergistic high affinity binding with
247 ATP (44, 45). Whether other kinases have such pseudosubstrate inhibitors that display this
248 synergistic high-affinity binding with ATP is not clear, although two of the most important
249 biological inhibitors of the PKA C-subunit, PKI and R1 α , show this property, while RII subunits of
250 PKA are actually substrates and not pseudo-substrates. The difference between substrate
251 inhibitors and pseudo-substrate inhibitors is fundamental. Do other kinases have physiologically
252 relevant pseudo-substrate inhibitors that binding with high affinity?

253 The specific features that convey high affinity binding to PKI are the amphipathic helix
254 that docks into a hydrophobic groove on the C-Lobe while the high-affinity binding of R1 α is due
255 to the first CNB domain (46, 47), CNB-A, which docks onto the Activation loop and the α G-helix.
256 These docking sites can be thought of as substrate tethering sites. While ATP binds with a 15
257 μ M affinity (K_m) when phosphorylating a small peptide, such as Kemptide (G-R-R-G-S-L), in the
258 presence of PKI or IP20 (residues 5-25) it binds with an affinity of \sim 60 nM. Similarly, IP20 on its
259 own has an affinity of \sim 200 nM, while in the presence of MgATP the affinity is \sim 1 nM. This high-
260 affinity synergistic binding also requires two Mg²⁺ ions that bind to the phosphates of ATP and
261 neutralize the negative charge of the phosphate (45), which allows the N- and C-lobes to fully
262 close. In the fully closed conformation F54 in the G-loop is adjacent to F187 that follows the
263 DFG motif. In this structure the γ -PO₄ is well shielded from water, a phenomenon which is
264 thought to facilitate the transfer of the phosphate (**Figure 5**). The second Mg²⁺ ion, in particular,
265 bridges the D184 in the C-Lobe with K72 in the N-Lobe. allowing for full closure of the catalytic
266 cleft. These unique features of IP20 allowed us to trap the fully closed conformation in our first
267 structures of the PKA catalytic subunit (5).

268
269 **Capturing Dynamics.** Identifying allosteric sites that lie distal to the catalytic site where
270 phosphoryl transfer takes place is one of the most important challenges facing the kinase
271 signaling community, as these sites which may be only transiently sampled, can nevertheless
272 be excellent therapeutic targets. While crystal structures and cryoEM structures provide us with
273 high-resolution portraits of folded proteins, these structures are static snapshots. In contrast,

274 NMR provides a residue-specific window into dynamics. NMR studies of the PKA C-subunit, first
275 described three states that are associated with the fully phosphorylated protein - uncommitted,
276 committed and quenched states (48). It should be emphasized that these states are all active
277 conformations where the R-spine is intact; they simply correlate with the opening and closing of
278 the active site cleft. The apo state, which is in an open conformation, is uncommitted to catalysis
279 while the binding of nucleotide, which completes the C-Spine, commits the kinase to catalysis.
280 The intermediate states with bound nucleotide correspond to partially closed states where the
281 C-terminal tail and the G-loop are still dynamic. How these states correlate with the
282 “Communities” of the kinase core was demonstrated by McClendon, et al (49). The quenched
283 and fully closed conformational state is captured when both ATP and the pseudo-substrate,
284 IP20, bind with high affinity. While these initial NMR studies captured the backbone dynamics, it
285 is the side chains that report much of the entropy-driven dynamics (10), and to explore this
286 hydrophobic space required labeling the side chains. When side chains (Val, Leu, and Ile) were
287 labeled, one could for the first time observe the correlated motions of the hydrophobic core
288 architecture, which experimentally captured the entropy-driven allostery (50).

289 Defining and targeting the allosteric sites of protein kinases is a holy grail, and if we
290 delve into the architecture of the kinase core as well as the tails and domains that flank the
291 kinase core in the PKA C-subunit, there are many sites where the core can become “uncoupled”
292 from the flanking motifs. Within the core, many sites lie distal to the active site that can uncouple
293 ATP and peptide/protein binding. Which of these mechanisms can abolish the synergistic high-
294 affinity binding of ATP and IP20 or can all of them do it? Some of these “uncoupling motifs” such
295 as F327, Y204, and E230 are sites that we have experimentally queried, whereas others such
296 as W196R, L205R, and E31V are known disease mutations that correlate with Cushing’s
297 Syndrome (51-55).

298 E230 is a critical residue for recognizing the P-2 arginine in PKA substrates. It couples
299 the peptide to Y204 in the P+1 loop and to E170 in the Catalytic loop. The E230Q mutant
300 uncouples the N- and C-lobes by “freezing” the enzyme into a stable open conformation that
301 can no longer bind ATP (56). Y204 is an example of an allosteric site that is not associated with
302 a change in conformation following replacement with Ala. Functionally this mutation reflects
303 instead an inability to transfer the γ -phosphate of ATP to a protein substrate while it is still fully
304 capable of transferring the γ PO₄ to water. Even though there is not a change in structure in the
305 Y204A mutant, mechanistically the Y204A mutation reflects a change in dynamics that can lead
306 to significant changes in the communities that the residue interacts with. Although changes in
307 dynamics can be captured and validated by NMR, changes in dynamics that lead to changes in

308 stability can also be predicted by LSP alignment. LSP alignment identified this mutation, Y204A,
309 as part of a dynamics-driven allosteric mechanism that can be described as a “Violin” model that
310 draws an analogy between distribution of thermal vibrations in proteins to vibrational patterns in
311 a violin (18, 57-59).

312 F327, which lies outside the kinase core, highlights another unique feature of PKA that is
313 conserved in all the AGC kinases (16). F327 is part of a C-terminal tail that wraps around both
314 lobes of the kinase core and is an essential feature of the ATP binding site (**Figure 5**). When all
315 of the residues comprising the hydrophobic shell around the adenine ring of ATP were mutated
316 to alanine, and analyzed in a yeast screen, only two were found to block viability, F327 and
317 L173 (60). We now know that L173 is a C-spine residue, but F327 lies outside of the kinase
318 core. Nevertheless, it is absolutely essential for binding of ATP. Replacing F327 with alanine
319 reduces the K_m for ATP over 10-fold (~450 μM) and completely abolishes the high-affinity
320 binding of ATP.

321 Three Cushing syndrome mutations were also shown to “uncouple” high-affinity binding
322 of inhibitor proteins. L205R uncouples binding of both RI and RII subunits as well as PKI by
323 disrupting binding to the P+1 pocket (55), while W196R disrupts binding to the cyclic nucleotide
324 binding domain (CNB-A) of both RI and RII subunits (51, 61). E31V is an example of a mutant
325 that uncouples the αA -Helix from the Activation loop, and this mutation also abolishes the
326 synergistic high-affinity binding of ATP (53). Paul Herman identified a set of mutants on the C-
327 lobe of the C-subunit that selectively enhanced the docking of protein substrates (23, 24). He
328 defined these as tethering sites, and all of these are directly linked to the $\alpha\text{F}/\alpha\text{E}$ -Helices. So,
329 there are a number of ways that one can uncouple the synergistic high-affinity binding of ATP
330 and IP20 or $\text{RI}\alpha$ by mutating sites that are distal to the catalytic site.

331
332 **F100A mutation highlights the importance of the αC - β4 Loop.** Another mutation that lies in
333 the αC - β4 loop, F100A, was recently described (23, 24). Adjacent residues in the αC - β4 loop
334 (V104I, L103F/I, and P101A) are actually oncogenic mutations in several protein kinases,
335 including PKA although none of these have been validated. The synergistic binding of ATP and
336 IP20 was completely abolished for the F100A mutant; even though the K_m s for Kemptide and
337 ATP for the F100A mutant were similar to the wild type (wt) C-subunit (62). Peptide assays are
338 a good way to evaluate the kinetic machinery of a protein kinase, and biochemically, based on
339 the Kemptide peptide assay, the kinetic mechanism for the C-subunit was not altered
340 significantly by the F100A mutation. However, the peptide assay does not reflect how a protein
341 kinase works in cells where it phosphorylates other proteins, not peptides. One will never

342 replicate Michaelis Menton kinetics in cells where the assay depends on having a large excess
343 of a small peptide substrate. This is, of course, relevant for peptides or hormones binding to a
344 receptor on the surface of the cell, but inside cells the protein substrates are not typically in
345 huge excess of the kinase and the interactions are not diffusion limited. They are instead
346 dependent on co-localization where the protein substrate is tethered in close proximity to the
347 kinase. This can be achieved by tethering directly to sites such as those described by Paul
348 Herman on the C-Lobe of the PKA kinase core (23, 24) or by binding to a kinase scaffold protein
349 in a way that brings the P-site close to the active site of the kinase (63). With this mechanism
350 protein phosphorylation is not diffusion-limited; however, it still highly depends on Brownian
351 Dynamics (BD) (64, 65); the charged residues are now simply tethered in close proximity to the
352 active site.

353 The importance of the α C- β 4 loop was actually initially hinted at by computational
354 analyses that involved Markov State modeling and NMR-restrained replica-averaged
355 metadynamics (RAM). These analyses suggested that there may be a flip of the α C- β 4 loop in
356 the apo protein and in the mutant (62). As seen in **Figure 4**, no such flip has been observed so
357 far in any of the crystal structures of the C-subunit to date (wt, E230Q, unphosphorylated C, and
358 the apo C-subunit), regardless of closed or open conformation. The subsequent NMR studies of
359 the F100A mutant also highlighted V104 and I150 as critical residues. I150 is a critical part of
360 the hydrophobic core architecture of the C-Lobe that anchors the α E Helix to the C-spine (L172
361 and I174 in β 7) and to L167 and P169 in the Catalytic loop (see above discussion and **Figure 2**).
362 In contrast, V104, which is part of the α C- β 4 loop, is one of three shell residues (SH1, SH2, and
363 SH3) that flank the R-spine residues in the N-lobe and V104 also touches ATP (25). Specifically,
364 one of the methyl side chains of V104 touches the adenine ring of ATP so it is one of the N-lobe
365 adenine capping residues for ATP (60) (**Figure 5**). All of the adenine capping residues in the C-
366 subunit come from the N-Lobe and the C-tail except for L173, which is the only capping residue
367 that comes from the C-Lobe. The C-spine is so important, because it links all of the hydrophobic
368 capping machinery in the N-Lobe with the hydrophobic core architecture in the C-Lobe. This
369 residue is not always conserved as a valine, but it is typically a small hydrophobic residue. This
370 hydrophobic residue also touches the well-studied gate-keeper residue, which in PKA is M120;
371 the gatekeeper is another shell residue (SH3) (66, 67).

372 The long computational studies (2 μ sec) carried out by Veglia predicted that the α C- β 4
373 loop undergoes a flip in the apo state, while the ITC results showed that the F100A mutant is
374 also more stable than wt C-subunit. Most importantly, the biochemical studies clearly
375 demonstrate that this mutation disrupts the synergistic binding of ATP and IP20. We thus asked

376 whether LSP could identify changes in dynamics that correlate with the NMR results. Could the
377 LSP analysis, which requires relatively short simulation times, predict residues or regions in the
378 C-subunit that could account for enhanced or reduced stability that results from this mutation
379 even if they cannot predict a conformational change?

380

381 **Comparing the LSP alignment of F100A with wt C-subunit.** Local Spatial Pattern (LSP)
382 alignment is a computational method developed in our laboratory for capturing conserved
383 patterns formed by C α -C β vectors in proteins (**Figure 6A**). Initially, it was utilized to identify
384 conserved hydrophobic ensembles in protein kinases (8, 9). More recently, this technique was
385 applied to Molecular Dynamics (MD) simulations, in an effort to analyze stable regions in Protein
386 Kinase A (68). By comparing spatial patterns formed by C α -C β vectors in differing
387 conformations generated via MD simulation it is possible to analyze thermal vibrations of
388 residues. These motions occur on a sub-nanosecond timescale and are considered to be the
389 foundation of dynamics-driven allosteric effects, which were predicted by Cooper and Dryden in
390 1984 (69) and have been observed in multiple proteins (70, 71).

391 LSP-alignment is a graph-theory based method that implements a Protein Residue
392 Network (PRN) approach (72). As we demonstrated, two major centralities of such PRNs can
393 contain important information on the local stability (Degree centrality, DC) and global
394 connectivity (Betweenness centrality, BC) of the protein (68) (**Figure 6B**). Our purpose here
395 was to identify changes in LSP-based PRNs associated with the F100A mutation, specifically
396 assessing whether these changes relate to the dynamic features of the α C- β 4 loop and
397 correlate with the NMR results. **Figure 6C** shows the corresponding PRNs laid out by the
398 ForceAtlas2 algorithm (73). This algorithm treats the weights assigned to edges as attractive
399 forces that balance the imposed repulsion of the nodes. In LSP-based PRNs, compact and
400 highly interconnected nodes correspond to more ordered regions of the protein where C α :C β
401 vectors move cohesively and preserve their mutual orientations. Both PRNs showed very similar
402 general structures, featuring dense groups of residues that correlate with the N and C-lobes.
403 These are linked by the Hinge, α C- β 4 loop and α C-helix. The analysis also includes the ATP
404 molecule, that was described by N1-C8 vector. Notably, the darker color of the α C- β 4 loop
405 residues in the F100A mutant indicates the increased level of BC.

406 To analyze changes of BC and DC in more detail we plotted them on scatterplots
407 (**Figure 7**). Residues from the α F-helix have the highest levels of DC in both the wt C-subunit
408 and F100A. This is consistent with the fact that this helix is the most stable structural element of
409 the kinase core and is known to be a major scaffold for the catalytic machinery of these

410 enzymes (**Figure 1**) (9). Several of the α F helix residues such as D220, W221, W222 and L227
411 from the C-spine, score high for both DC and BC. This indicates that these residues act both as
412 hubs and connectors. The most significant change in the F100A mutant is the increase of BC for
413 the five residues from the α C- β 4 loop (highlighted in blue). Conversely, a set of highly
414 conserved residues (marked in red), previously noted for having the highest levels of BC (68),
415 show a reduction in their DC and this reduction is even more pronounced in the BC values in
416 the F100A mutant.

417 The detailed values of DC and BC changes associated with the F100A mutation are
418 shown in **Figure 8**. Since both of these parameters have positive and negative values, we
419 visualize them separately, mapping them onto the PKA structure. Positive changes in DC
420 correspond to areas that lose stability of their C α -C β vectors upon the mutation (**Figure 8A**, left,
421 red). These include the catalytic area of the kinase, and most importantly, universally conserved
422 K72, the DFG-motif, including D184, and the substrate binding site. Notably, the Δ DC value for
423 ATP is one of the highest (**Figure 8A**, center), indicating a significant loss of stability of the
424 adenine ring in the mutant. Negative changes in Δ DC (**Figure 8A**, right, blue) correspond to
425 areas of PKA that become more stable in the mutant. Significant changes were primarily
426 localized in the α C- β 4 loop. Similarly, negative changes in Δ BC values (**Figure 8B**, right, blue)
427 were also found in the α C- β 4 loop, signifying that the role of the major connecting area between
428 the lobes shifts from the catalytic area (**Figure 8B**, left, red) to this region. Overall, the F100A
429 mutation causes the rigidification of the α C- β 4 loop, especially V104 at the tip becomes more
430 stable and rigid following mutation of F100. Our analysis suggests that the major connectors
431 between the N- and C-lobes such as K72 from β 3 stand (N-lobe) and D184 from the DFG motif
432 (C-lobe) in the wt protein gets impaired and destabilized in response to the F100A mutation.
433 The rigidified α C- β 4 loop loses the dynamic coupling between the two lobes and the
434 connectivity between both lobes changes, as seen by V104 and I150, which become the major
435 connector points following the mutation. Overall, the mutation at the α C- β 4 loop changes the
436 allosteric communication between the two lobes.

437 In general, these results can be interpreted as a disruption of dynamic communication
438 between the two lobes where ATP binding in the N-Lobe comes together with the major catalytic
439 machinery in the C-Lobe (**Figure 2**). The prominent role of D184 in the C-lobe and K72 in the N-
440 Lobe, hallmark features of the conserved regulatory triad, are also altered. Upon the mutation, a
441 robustly stable region around F102-L106 becomes a dominant connector between the lobes,
442 leading to a significant disruption of correlated dynamics observable in the active site of the wt
443 C-subunit.

444

445 **Capturing side chain dynamics.** Our initial preliminary LSP alignment comparison of wt C-
446 subunit in the presence of ATP with the F100A mutant indicated significant destabilization of the
447 entire catalytic machinery in the C-lobe in parallel with enhanced stability of the α C- β 4 loop, a
448 node in the C-tail and the α H- α I loop (**Figure 8A**). While a much more extended analysis is
449 needed to validate the LSP predictions, the overall results clearly show that the dynamic
450 features of the α C- β 4 loop have changed in the F100A mutant. As discussed earlier and as
451 indicated in **Figure 4**, we did not see significant changes in the α C- β 4 loops when we compared
452 our various crystal structures, which included open and closed conformations of the active
453 kinase as well as an inactive unphosphorylated C-subunit. Specifically, the tip of the α C- β 4 loop
454 remained anchored to the α E Helix in all of these structures. Intrigued by our LSP results with
455 the F100A mutant, we thus looked more carefully at the side chain residues in the α C- β 4 loop in
456 our various structures. We asked specifically if there were differences in any of the side chain
457 residues that could be predictive of subsequent conformational changes in the backbone as was
458 predicted by the NMR studies. The side chains of the α C- β 4 loop in the ternary complex with
459 ATP and IP20 are shown in **Figure 9A**, and no significant differences were seen for the E230Q
460 mutant and the unphosphorylated C-subunit. In this structure the side chain of K105 was
461 toggling (\sim 4.6Å) between two carboxyl groups (E107 and E121), and its backbone carbonyl (the
462 first residue of β 4) is hydrogen bonded to the backbone amide of E121 (the last residue of β 5)
463 (**Figure 9B**). While the apo protein showed no major changes in the backbone of the α C- β 4
464 loop, the side chain of K105 has flipped and is now interacting with carbonyls in the β -turn
465 residues. It is also close to the side chain of N99. Based on the crystal structures, this space is
466 not sampled by K105 in the wt C-subunit; instead this space is filled by ordered water molecules.

467 To look more carefully at the space that is sampled by the side chain of K105, we looked
468 at the MD simulations that were used for the LSP analysis of the wt binary complex of the C-
469 subunit and the F100A mutant. As seen in **Figure 10A**, for the wt C-subunit there is one global
470 energy minimum, and the predominant structure for the global energy minimum correlates well
471 with our structure of the ternary complex (**Figure 9A**). Based on the simulations, however,
472 instead of toggling between E107 and E121, the side chain of K105 interacts predominantly with
473 the side chain of E107 (**Figure 10C**), while it rarely samples the side chain of E121 (**Figure**
474 **10D**). In contrast to the wt C-subunit and the apo protein, the mutant shows two energy basins
475 (**Figure 10B**). The minor local minimum corresponds closely to the wt C-subunit with K105
476 interacting with E107. In contrast, the major global energy minimum shows the side chain of

477 E105 interacting with the side chain oxygen of N99 and far from the side chain of E107. The
478 probability distribution of this interaction with N99 is shown in **Figure 10E**, which confirms that
479 the mutant has a stronger propensity to interact with N99. As discussed above, N99 is thought
480 to be a critical residue based on the importance of the homologous residue in BRaf (R509) for
481 dimerization and because the backbone of this residue is always anchored to a key residue in
482 the α E Helix (Y156) in every kinase. To interrogate the strength of the Y156 hydrogen bond to
483 the backbone amide of N99, we also looked at its probability distribution in the simulations
484 (**Figure 10F**). While the H-bond is strong in the complex and in the mutant, it is surprisingly
485 destabilized in the apo structure.

486 After investigating the binary complex of the C-subunit for both wt and F100A, we next
487 analyzed the ternary complex. Using the MD simulations, we asked specifically if the F100A
488 mutation alters the dynamic properties of K105 when both ATP and PKI are present. The free
489 energy landscape (**Figure 11**) depicts the overall energy profile for the wt ternary complex and
490 the F100A mutant. The wt ternary complex, in general, behaves similarly to the binary complex.
491 Both exhibit a single global energy minimum (**Figure 11A**). In contrast, the F100A mutation
492 shows enhanced dynamics for both binary and ternary complexes, although there are multiple
493 energy basins in the ternary complex (**Figure 11B**). The side chain dynamics of K105 also show
494 different interaction profiles (**Figures 11 C, D and E**), and differences are seen even when just
495 the binary and ternary complexes are compared. In the wt binary complex, the side chain of
496 K105 predominately interacts with the side chain of E107 (**Figure 10C**) and interacts more
497 transiently with the side chain of N99 (**Figure 10E**). This is in contrast to the wt ternary complex
498 where the interactions of K105 and N99 side chains increase (**Figure 11E**), while the interaction
499 with E107 decreases (**Figure 11C**). The side chain of K105 in the wt binary, ternary, and apo
500 states rarely samples the side chain of E121 (**Figures 10D and 11D**). The hydrogen bond
501 between Y156 and N99 is also maintain in the binary and ternary complexes, but broken in the
502 apo protein (**Figures 10F and 11F**).

503 Does the F100A mutation introduce additional changes in the crosstalk of the ternary
504 complex? The major difference is between K105 and E121, which correlates with the primary
505 energy minimum (**Figure 11D**). This interaction is not seen in any of the other complexes. In
506 addition, the side chain of K105 has a reduced propensity for interacting with the side chain of
507 E107 as shown in the second local minimum. Finally, there are no significant changes between
508 Y156 and the backbone amide of N99 in the mutant (**Figure 11F**). Hence, the enhanced side

509 chain dynamics of K105 have been observed following the F100A mutation where the side of
510 K105 toggles between E121 and N99, and to some extent E107 (**Figure 11G**). In general,
511 these results agree with the NMR experimental results and suggest that the F100A mutation
512 alters the dynamic interactions of the α C- β 4 loop, leading to the hypothesis of the disruption in
513 the allosteric communication between both lobes.

514 The most striking difference, based on the MD simulations, is the enhanced interaction
515 of K105 with the side chain of E121, a key residue that binds directly to the adenine ring of ATP.
516 As seen in **Figure 12A**, in the crystal structure of the ternary complex the backbone amide of
517 E121 hydrogen bonds to the backbone carbonyl of K105, while the backbone carbonyl of E121
518 hydrogen bonds directly to the adenine ring of ATP. The hydrophobic packing between the ATP
519 adenine ring and V104, a shell residue, is extended to the R-spine residues, L95 (RS3) and
520 L106 (RS4), which is also highlighted. How these predicted changes in dynamics in the F100A
521 mutant correlate with enhanced stability and/or alter function need to now be validated
522 experimentally.

523 **Summary and future directions.** Based on the NMR analysis of the F100A mutant, we more
524 rigorously examined the α C- β 4 loop showing first how it is firmly anchored to the hydrophobic
525 core architecture of the C-lobe. In addition, we reviewed the synergistic high-affinity binding of
526 ATP and PKI, a phenomenon that was described in detail many decades ago for PKI but never
527 fully explained in terms of its mechanism. In the F100A mutant, this synergy is uncoupled.
528 Finally, given that both NMR and the Markov State model suggested changes in the α C- β 4 loop,
529 we carried out an LSP analysis of the mutant. The LSP analysis correlated remarkably well with
530 the NMR predictions. To explain this correlation, we compared various crystal structures of the
531 C-subunit to see if we could detect differences in side chain dynamics since the backbone did
532 not change significantly. LSP alignment is a tool that is perfectly poised to detect alterations in
533 side chain dynamics as it identifies differences in the geometry of the α carbon/ β carbon vectors
534 (**Figure 6**), a property that likely precedes any conformational changes, which take a much
535 longer time to simulate with classical Molecular Dynamics. MD simulations of the binary and
536 ternary complexes of the wt C-subunit, the F100A mutant and the apo C-subunit were also used
537 to explore changes in side chain dynamics.

538 Although in these short MD simulations we did not detect a flip of any backbone residues
539 in the α C- β 4 loop, we did see significant differences in the side chain dynamics of K105 in the
540 structure of the apo protein. This could, in principle, correlate with a weakening of the β -turn.

541 Based on the MD simulations, the side chain of K105 is also flipped in the F100A mutant. In
542 both cases the side chain of K105 is exploring the space that is occupied by the ordered water
543 molecules in the other structures. These water molecules play an essential role in stabilizing the
544 β -turn motif. We thus predict that the enhanced flexibility of the side chain of K105 may be an
545 initial step that leads to subsequent changes in the backbone dynamics. This prediction needs
546 now to be validated with crystal structures to see if the mutation actually “freezes” an altered
547 conformation of the α C- β 4 loop. The potential importance of both N99 and K105 in mediating
548 changes in dynamics also needs to be experimentally validated biochemically, by NMR, and by
549 further computational analyses. We predicted that N99 is important due to its conserved
550 hydrogen bonding to Y156 and the conserved packing of the side chain of Y156 with
551 hydrophobic residues in the β -turn. This, however, is the first potential indication of a direct role
552 for K105. The graphs of the hydrogen bond between the side chain of Y156 and the backbone
553 amide of N99 show that this bond is very stable in the binary and ternary complexes and in the
554 mutant but weakened in the apo protein (**Figure 10E**), and this would also be consistent with
555 the prediction that the β -turn may be more flexible in the absence of ligands but stabilized in a
556 different way in the F100A mutant.

557 Overall, our work suggests that the α C- β 4 loop should be carefully examined in all
558 protein kinases as it is a focal point for linking ATP binding to peptide/protein binding and for
559 opening and closing of the catalytic cleft. Our early structure captured the high affinity binding of
560 both ATP and IP20, a pseudo-substrate inhibitor, in a fully closed conformation (**Figure 12B**). In
561 this conformation the IP20 peptide is firmly anchored to the catalytic machinery of the C-lobe,
562 while F327 and Y330 in the C-terminal tail are anchored to ATP. The side chain of the P-3
563 arginine in IP20 interacts directly with ATP, E127, and Y330 in the C-terminal tail, and all are
564 close to the α C- β 4 loop. This convergence of the P-3 arginine side chain with Y330 may explain
565 the enhanced synergy that is seen when the PKA C-subunit interacts with its pseudo-substrate
566 inhibitors, PKI and RI α , and understanding this synergy is a major future challenge. E127 binds
567 to the other ribose hydroxyl moiety. E121 and E127 flank the linker that joins the N- and C-lobes
568 (**Figure 12A**), and this linker is likely a critical feature for opening and closing of the active site
569 cleft. K105 in the α C- β 4 loop can obviously sense differences in the apo, binary and ternary
570 complexes, and can also sense mutations. This space now needs to be further explored. The
571 α C- β 4 loop is also a good potential therapeutic target as the specific residues such as N99 and
572 K105 that are mechanistically important are different in all kinases in contrast to the conserved

573 residues such as K72 and D184 that position the phosphates of ATP. The importance of α C- β 4
574 loop is also reinforced because the cancer mutations are located here (29).

575 Finally, given the extremely close correlation of the LSP analysis with the NMR results
576 and the Markov State model predictions, as well as our principal component analysis (PCA) of
577 the wt and F100A mutant, we suggest that LSP could be used as a predictor of dynamics for
578 any mutant or even for carrying out an alanine scan of any protein. These sites could then be
579 examined experimentally. Although purifying these proteins and especially labeling the
580 hydrophobic side chains is not only a major time investment but also very expensive, these
581 methods are essential to experimentally validate the importance of hydrophobic residues in
582 mediating entropy-driven allostery. In contrast, LSP is rapid and relatively inexpensive and could
583 easily be used as an initial screen to identify potentially important residues that contribute to
584 dynamics.

585

586 **Material and Methods**

587 **Molecular Dynamic (MD) Simulation.** The catalytic subunit of PKA was prepared using the
588 crystal structure (PDB: 1ATP) (5) for all-atom MD simulations using the AMBER16 suite (74). In
589 order to study the allostery dynamics of the α C- β 4 loop and compare the effect of mutation of
590 F100A on structure-dynamics of the catalytic subunit, we prepared three systems: The wt C-
591 subunit (ATP/Mg²⁺) where Mn²⁺ ions were replaced with Mg²⁺ and removed the PKI to form a
592 binary complex. In addition, we kept the PKI along with the ATP to form a ternary complex
593 (ATP/Mg²⁺/PKI); the F100A mutant structure in both the binary and ternary complex by replacing
594 the Phe100 to Ala, and allowing the side chains to be added by the program LEaP module in
595 AMBER, and the Apo system, which was prepared by taking the coordinates from the PDB:
596 1J3H (75). Amber ff14SB (76) force field was used to describe proteins. Titratable residues
597 were protonated at pH 7.0 based on PROPKA3.0 (77, 78). Parameters for ATP and Mg²⁺ were
598 obtained from the Bryce Group AMBER parameters database (79, 80). The phosphorylated
599 serine and threonine residues were described using the phosaa10 force field (81). The
600 hydrogens and counter ions were added, and the system was solvated in the octahedron
601 periodic box using the TIP3P (82) water model and 150 mM NaCl with a 10 Å buffer in AMBER
602 tools. Systems undergo minimization, heating, and equilibration steps using the AMBER16.
603 Initially, systems were minimized by 1,000 steps of hydrogen-only minimization, 2,000 steps of
604 protein and ligand minimization, 2,000 steps of side chain minimization, 2,000 steps of
605 backbone minimization, and followed by removing all restraints for 5,000 steps of all-atom

606 minimization. Systems were gradually heated from 0° to 300° K over 50 ps with 2-fs time-steps
607 and 10.0 kcal mol⁻¹Å⁻² position restraints on the protein. The temperature was maintained by the
608 Langevin thermostat (83, 84) while the pressure was maintained using the Barendsen barostat
609 (85). Constant pressure equilibration with a 10 Å non-bonded cutoff with Particle Mesh Ewald
610 (PME) (86) was performed with 1000 ps of unrestrained equilibration. Production simulations
611 were performed on Graphic Processing Unit-enabled AMBER16 as above in triplicate for 200 ns
612 each for an aggregate of 600 ns. Overall, 60,000 snapshots were generated for each system
613 and saved for analysis.

614
615 **LSP-alignment based Protein Residue Networks.** LSP-based PRNs were built as described
616 earlier (68). Five 10 ns intervals were taken from a 200 ns trajectory at specific intervals: 0-10
617 ns, 50-60 ns, 90-100 ns, 130-140 ns, and 170-180 ns. From each interval, 100 structures were
618 extracted with a step of 0.1 ns. The LSP-alignment between each set of 100 structures was
619 performed in an all-to-all manner. The resulting adjacency matrices were averaged for each set.
620 Degree centrality and betweenness centrality were calculated for five average matrices. Finally,
621 five values for the centralities were averaged, and the standard error of the mean was
622 calculated.

623
624
625 **Principal Component Analysis (PCA) and Free Energy Landscape (FEL).** PCA is a broadly
626 used method to extract the slow and functional motions of biomolecules (87-89). First, the
627 covariance matrix, C, was calculated based on the fluctuations of the Ca
628 atom of each residue. The elements C_{ij} in the matrix were obtained from the fluctuation of amino
629 acids and diagonalized as given in Equation 1

630
631
$$C_{ij} = \langle (x_i - \langle x_i \rangle) (x_j - \langle x_j \rangle) \rangle \quad (1)$$

632
633 where x_i and x_j are the i^{th} or j^{th} atom coordinates and $\langle x_i \rangle$ and $\langle x_j \rangle$ represent the mean average
634 coordinate of the i^{th} or j^{th} atom, respectively. The principal components (PCs) will be obtained by
635 diagonalizing the covariance matrix C. The corresponding eigenvalues and eigenvectors were
636 calculated.

637

638 The Free Energy Landscape (FEL) can be drawn based on PCA as a reaction coordinate using
639 the Equation 2 (90, 91)

640

$$641 \quad G_i = -k_B T \ln \frac{N_i}{N_m} \quad (2)$$

642 where k_B represents the Boltzmann constant and T represents the absolute temperature. N_i and
643 N_m are the i^{th} bin populations and the maximum populated bin, respectively.

644

645

646 **Acknowledgments.** This work was supported by the National Institutes of Health, GM100310
647 and HL144130 to G.V, and GM130389 to S.S.T.

648

649 **Conflict of interest.** The authors declare no conflict of interest.

650

651 **Author contributions.** J.W. and S.S.T. reviewed the hydrophobic core architecture literature.
652 J.W., N.A.J., C.O., G.V., A.P.K., and S.S.T. contributed to the design of F100A analyses. J.W.,
653 N.A.J., C.O., G.V., A.P.K., and S.S.T. contributed to the critical analysis of the data and writing
654 of the manuscript. N.A.J. and A.P.K. performed the MD simulations and LSP analysis. J.W.,
655 A.P.K. and S.S.T. contributed to the formatting of the text and preparing figures. S.P.H., C.O.,
656 and G.V. contributed to the editing of the manuscript. All authors have given approval to the final
657 version of the manuscript.

658 **FIGURE LEGENDS.**

659 **Figure 1. Hydrophobic α F-helix serves as a central scaffold.** (A). α F-helix is very
660 hydrophobic and creates an interface with multiple motifs including the Catalytic machinery
661 (colored in tan) and tethering sites (in sand) of PKA C-subunit. Two key charged residues, D220
662 and E230, sit at the two ends of α F-helix. (B). α F-helix is a central scaffold for assembly of the
663 entire molecule. D220 forms two H-bonds to Y164 and R165 of YRD motif, and E230 salt-
664 bridges to P-2 Arg of PKI. (C). Sequence alignment of α F-helix segment of PKA with other
665 kinases. All share a very hydrophobic helix, the highly conserved residues, D220 are colored in
666 red and E230 in red box.

667 **Figure 2. Hydrophobic interface anchors the Catalytic machinery to the α E-helix and α F-**
668 **helix.** (A). I150 (in red) from α E-helix plays an important role by docking to α F-helix and
669 Catalytic loop. Three residues from β 7, L172, L173, and I174 (in dark tan) assemble the
670 hydrophobic surface from α E-helix to ATP pocket. L173 and I174 are part of C-Spine. R-spine
671 are also shown in red. D220 bridges H158 from α E-helix to YRD motif. (B). The logo of spines
672 shows how important those hydrophobic residues are. The sequence of β 6- β 9 segment is also
673 shown.

674 **Figure 3. The buried surface of α C- β 4 loop.** (A). α C- β 4 loop (in teal) in PKA links the N-lobe
675 to its C-lobe. The hydrophobic residues on the loop docks to α E-helix, F18 and L19 from α A-
676 helix and Y306 from C-tail are also part of this surface. F100 is colored in red. (B). The H-bond
677 network of α C- β 4 loop. Y156 from α E-helix H-bonds to N99 backbone amide. Three water
678 molecules also help to nucleus the network. (C). Sequence alignment of α C- β 4 loop of PKA with
679 other kinases. The highly conserved residues are highlighted, E91 colored in red, L95 and L106
680 in red box.

681 **Figure 4. α C- β 4 loop is a very stable element.** (A). Hydrophobic surface of α E-helix which
682 anchors to α C- β 4 loop, α F-helix and tethering sites. (B). Superimposition of α C- β 4 loop in
683 structures of PKA and other kinases. α C- β 4 loop is very stable, not only in different
684 conformations of PKA, but also in other kinase structures including active and inactive Src. (C).
685 Sequence alignment of α E-helix of PKA with other kinases. Y156, in red box, is highly
686 conserved.

687 **Figure 5. Hydrophobic residues play key roles in PKA.** (A). High-affinity binding of PKI is
688 mediated by the hydrophobic surface of an amphipathic helix and P+1 inhibitor site, both
689 highlighted in red. The sequence of PKI is also shown. (B). Hydrophobic interface between the
690 α E and α F-helices. One side of α F-helix (in red) is shown in tan, and another side in sand,
691 which is the same color coding as Figure 1A. (C). Hydrophobic pocket surrounding ATP. L172,
692 L173, and I174 from β 7 anchor this ATP pocket to α E-helix. F327 from C-tail is highlighted in
693 red.

694 **Figure 6. Local Spatial Pattern (LSP) alignment method.** (A). Spatial patterns detected by
695 the LSP-alignment are formed by α C- β vectors. Both mutual positions and orientation in space
696 of these vectors are taken into account. (B). Two major centralities that characterize graphs.
697 Degree centrality (DC) is the sum of connections for each node. The highlighted node in the
698 middle has the highest DC value of 8. Residues with high level of DC are local "hubs".
699 Betweenness Centrality (BC) of a node is the number of shortest paths between all other pairs
700 of nodes that pass through this node. Two highlighted nodes are the main connectors in the

701 graph with BC equal to 6. Residues with high level of BC are global connectors between local
702 hubs. (C) Visualization of Protein Residue Networks (PRNs) of PKA before and after the
703 mutation laid out by Gephi software package using ForceAtlas2 algorithm. The diameter of
704 nodes is proportional to the residues DC. Nodes with higher BC have darker color. Four
705 residues from the α C- β 4 loop (103-106) are highlighted by oval. The Hinge region is indicated
706 by the dashed oval.

707 **Figure 7. Distribution of Betweenness centrality vs. Degree centrality for PKA residues:**
708 **wt C-subunit (A) and F100A (B).** Residues with Degree centrality (DC) are local "hubs",
709 representing the most stable parts of the molecule. Residues with high Betweenness centrality
710 (BC) are global connectors and are "bottlenecks" between densely interconnected "hubs".
711 Residues of the central α F-helix are shown as brown circles. Their high levels of DC and BC
712 don't change upon the F100A mutation, meaning that the helix remains to be a central structural
713 element in the PKA mutant. Five residues from the α C- β 4 loop are highlighted as blue dots. The
714 significant increase in BC and a certain increase in DC shows that in the mutant this group of
715 residues becomes a significant point of connectivity between the kinase lobes. On the contrary,
716 the highly conserved residues highlighted as red circles show a drastic decrease in BC. Error
717 bars represent standard error calculated for five 10 ns trajectories.

718 **Figure 8. Changes of DC and BC in PKA upon F100A mutation.** The middle graphs
719 represent changes in the corresponding parameters. Positive changes are mapped on the PKA
720 structure (left) with dark red color corresponding to the maximum changes. On the right the
721 negative values of the changes are mapped on the structure to illustrate their distribution. Dark
722 blue color corresponds to the most negative values. Error bars represent standard error
723 calculated for five 10 ns trajectories. The secondary structure of PKA is shown on top of the
724 sequence axis for reference.

725 **Figure 9. Dynamic feature of K105 on α C- β 4 loop.** (A). In the wt PKA:ATP:Mg:PKI complex
726 structure, the side chain of K105 is likely interact with E107 and E121, and its main chain
727 carbonyl forms a H-bond to backbone amine of E121. (B). In the wt Apo PKA structure, the
728 K105 side chain interacts with β -turn, whereas its main chain carbonyl still H-bonds to backbone
729 amines of E107 and E121. The H-bonds are shown as dash line in black, and the non H-bond
730 are colored in green and the distance are labeled.

731 **Figure 10. Energy landscapes of wt C-subunit and F100A mutant in binary complex.** The
732 free energy landscapes (FEL) were generated based on the principal component analysis
733 (PCA) for the wt C-subunit (A) and F100A mutant (B). The H-bonds are shown in the black dash
734 line and the non H-bond in green along with the distance in Angstroms (Å). The probability
735 distribution plots for specific side chain dynamics are also shown; (C) K105 NZ to E107 OE2,
736 (D) K105 NZ to E121 OE2, (E) K105 NZ to N99 OD1, and (F) N99 N to Y156 OH. The
737 probability density function (PDF) is a relative measure of how densely data points are
738 distributed along the x-axis.

739 **Figure 11. Energy landscapes of wt C-subunit and F100A mutant in ternary complex.** The
740 free energy landscapes (FEL) were generated based on the principal component analysis
741 (PCA) for the wt C-subunit with PKI (A) and F100A mutant with PKI (B). The H-bonds are shown
742 in the black dash line and the non H-bond in green along with the distance in Angstroms (Å).
743 The probability distribution plots for specific side chain dynamics are also shown; (C) K105 NZ
744 to E107 OE2, (D) K105 NZ to E121OE2, (E) K105 NZ to N99 OD1, and (F). N99 N to Y156 OH.
745 (G) the enhanced side chain dynamics of K105 in the F100A ternary complex: the side chain of

746 K105 toggles to its neighboring residues, E121 (white, global energy minima), N99 (green, first
747 secondary minima), and E107 (sand, second secondary minima). The probability density
748 function (PDF) is a relative measure of how densely data points are distributed along the x-axis.

749 **Figure 12. High-affinity binding of ATP and PKI converge at the α C- β 4 loop.** (A). V104
750 in α C- β 4 loop (in teal) is hydrophobically anchored to the adenine ring of ATP. The main chain
751 carbonyl of K105 forms an H-bond to the backbone amide of E121, while its main chain
752 carbonyl hydrogen bonds to ATP. The distance between K105 and E121 side chains is
753 strengthened in the F100A mutant. Two spine residues, L95 and L106, in this loop are also
754 shown. The linker that joins the N- and C-lobes (red) is flanked by E121 and E127. (B).
755 Hydrophobic capping of the adenine ring of ATP is mediated mostly by N-lobe residues
756 including V104 in the α C- β 4 loop, as well as F327 in the C-terminal tail. In contrast, the P-3 to
757 P+1 peptide is anchored to the catalytic machinery of the C-lobe. By binding to L173 in the C-
758 lobe, the adenine ring completes the C-Spine, and thus fuses the adenine capping motif in the
759 N-lobe with the extensive hydrophobic core architecture of the C-lobe. In the fully closed
760 conformation, the side chain of Y330, also in the C-terminal tail, is anchored to the ribose ring of
761 ATP. The only direct contact of the peptide/catalytic machinery with the N-lobe is mediated by
762 the P-3 arginine which binds to the ribose ring of ATP and to E127 in the linker. In the fully
763 closed conformation the P-3 arginine also binds to the side chain of Y330 in the C-terminal tail.
764 Some of the mutations that disrupt the synergistic high-affinity binding of ATP and
765 peptide/protein (E230Q, Y204A, F327A, L173A, and E31V) are highlighted. The hydrophobic
766 residues in the amphipathic helix and P+1 inhibitor site of PKI are shown in red.

767

768 **REFERENCES.**

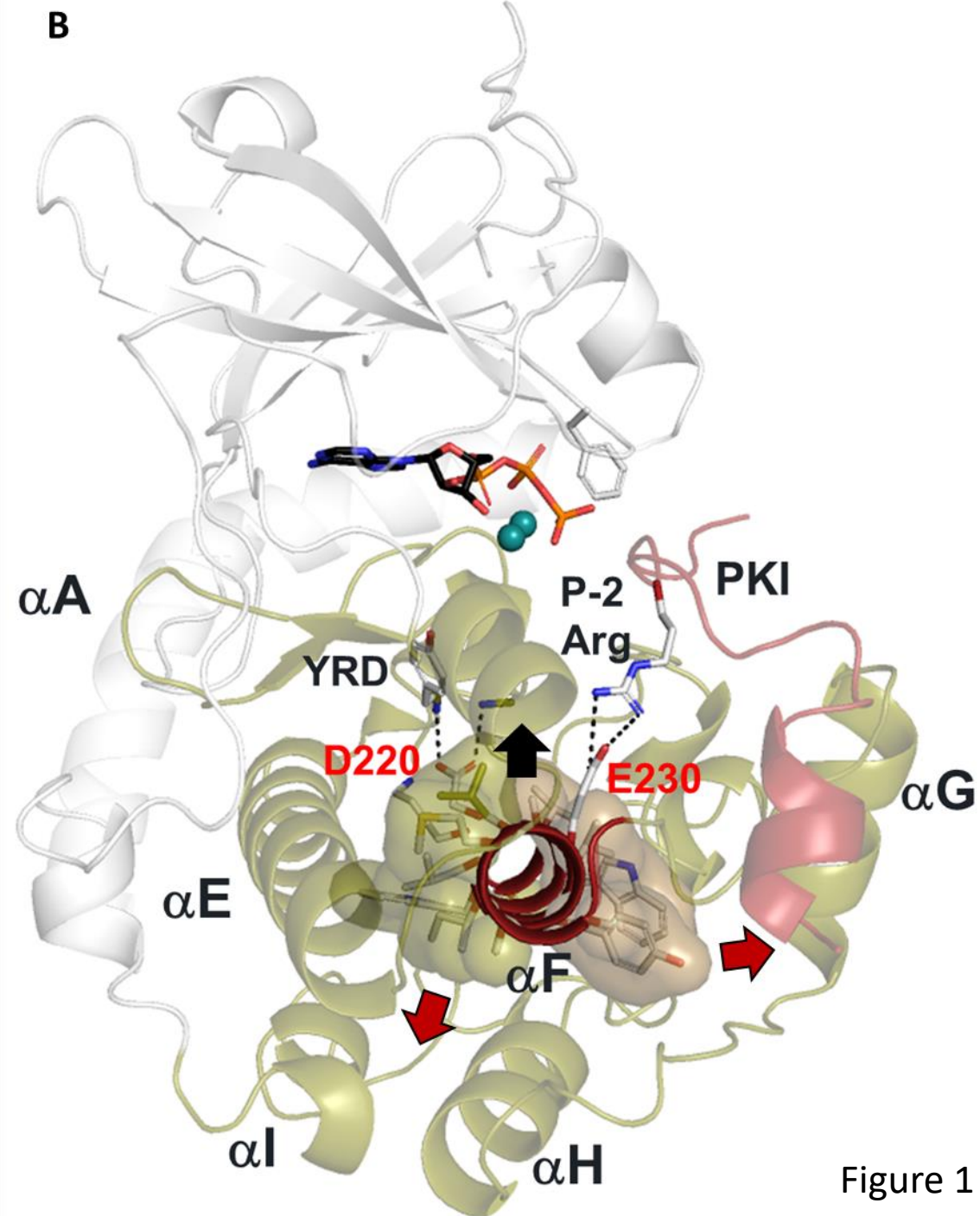
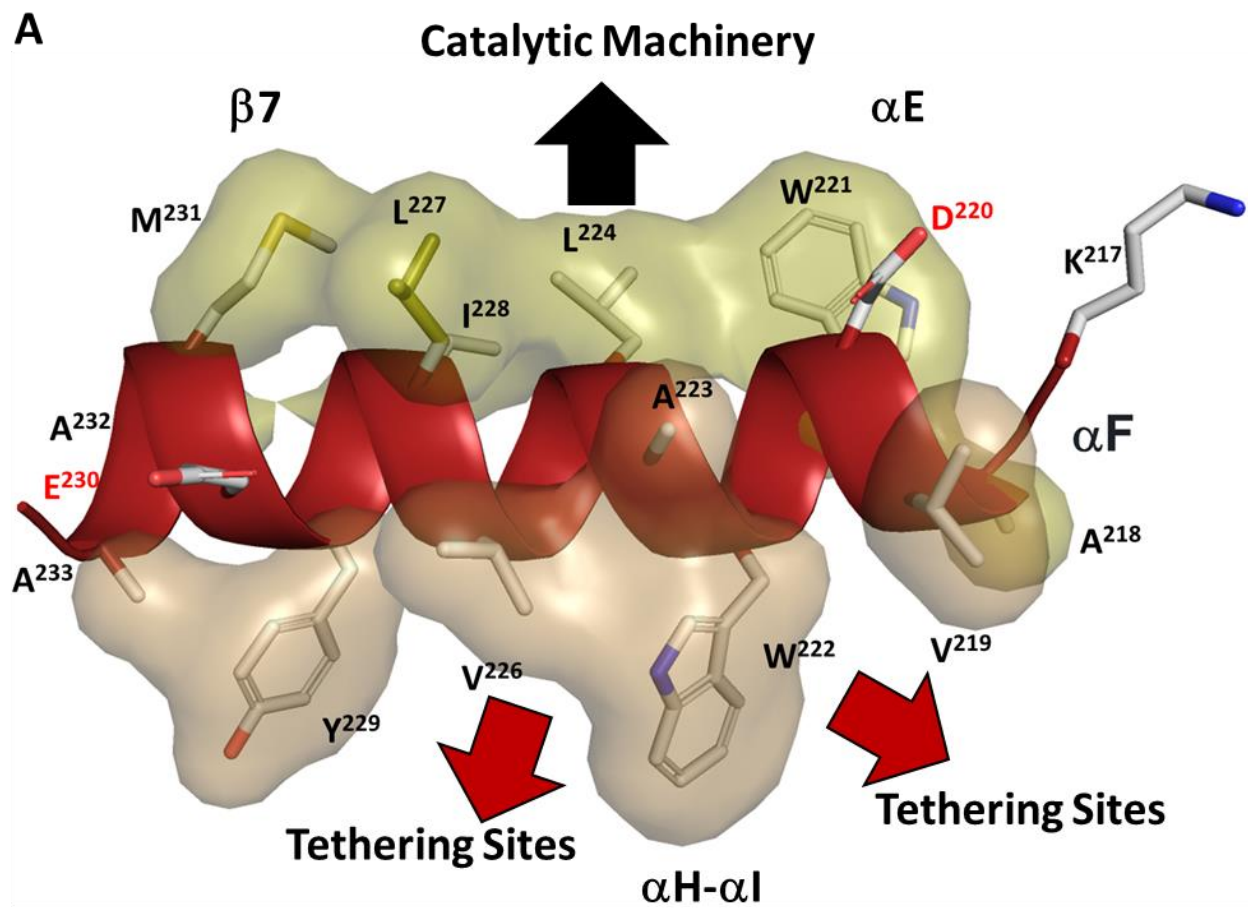
- 769
- 770
- 771 1. W. C. Barker, M. O. Dayhoff, Viral src gene products are related to the catalytic chain of
- 772 mammalian cAMP-dependent protein kinase. *Proc Natl Acad Sci U S A* **79**, 2836-2839
- 773 (1982).
- 774 2. S. K. Hanks, A. M. Quinn, T. Hunter, The protein kinase family: conserved features and
- 775 deduced phylogeny of the catalytic domains. *Science* **241**, 42-52 (1988).
- 776 3. D. R. Knighton, J. H. Zheng, L. F. Ten Eyck, V. A. Ashford, N. H. Xuong et al., Crystal
- 777 structure of the catalytic subunit of cyclic adenosine monophosphate-dependent protein
- 778 kinase. *Science* **253**, 407-414 (1991).
- 779 4. D. R. Knighton, J. H. Zheng, L. F. Ten Eyck, N. H. Xuong, S. S. Taylor et al., Structure of
- 780 a peptide inhibitor bound to the catalytic subunit of cyclic adenosine monophosphate-
- 781 dependent protein kinase. *Science* **253**, 414-420 (1991).
- 782 5. J. Zheng, D. R. Knighton, L. F. ten Eyck, R. Karlsson, N. Xuong et al., Crystal structure
- 783 of the catalytic subunit of cAMP-dependent protein kinase complexed with MgATP and
- 784 peptide inhibitor. *Biochemistry* **32**, 2154-2161 (1993).
- 785 6. D. Bossemeyer, R. A. Engh, V. Kinzel, H. Ponstingl, R. Huber, Phosphotransferase and
- 786 substrate binding mechanism of the cAMP-dependent protein kinase catalytic subunit
- 787 from porcine heart as deduced from the 2.0 Å structure of the complex with Mn²⁺
- 788 adenylyl imidodiphosphate and inhibitor peptide PKI(5-24). *EMBO J* **12**, 849-859 (1993).
- 789 7. D. A. Johnson, P. Akamine, E. Radzio-Andzelm, M. Madhusudan, S. S. Taylor,
- 790 Dynamics of cAMP-dependent protein kinase. *Chem Rev* **101**, 2243-2270 (2001).
- 791 8. A. P. Kornev, N. M. Haste, S. S. Taylor, L. F. Ten Eyck, Surface comparison of active
- 792 and inactive protein kinases identifies a conserved activation mechanism. *P Natl Acad*
- 793 *Sci USA* **103**, 17783-17788 (2006).
- 794 9. A. P. Kornev, S. S. Taylor, L. F. Ten Eyck, A helix scaffold for the assembly of active
- 795 protein kinases. *Proc Natl Acad Sci U S A* **105**, 14377-14382 (2008).
- 796 10. J. Kim, L. G. Ahuja, F. A. Chao, Y. Xia, C. L. McClendon et al., A dynamic hydrophobic
- 797 core orchestrates allostery in protein kinases. *Sci Adv* **3**, e1600663 (2017).
- 798 11. G. D. Rose, From propensities to patterns to principles in protein folding. *Proteins*
- 799 10.1002/prot.26540 (2023).
- 800 12. G. D. Rose, W. B. Young, L. M. Gierasch, Interior turns in globular proteins. *Nature* **304**,
- 801 654-657 (1983).
- 802 13. A. C. Newton, Protein kinase C: perfectly balanced. *Crit Rev Biochem Mol Biol* **53**, 208-
- 803 230 (2018).
- 804 14. S. S. Taylor, K. Soberg, E. Kobori, J. Wu, S. Pautz et al., The Tails of Protein Kinase A.
- 805 *Mol Pharmacol* **101**, 219-225 (2022).
- 806 15. J. H. Weng, C. R. Trilling, P. Kaila Sharma, E. Stormer, J. Wu et al., Novel LRR-ROC
- 807 Motif That Links the N- and C-terminal Domains in LRRK2 Undergoes an Order-Disorder
- 808 Transition Upon Activation. *J Mol Biol* **435**, 167999 (2023).
- 809 16. N. Kannan, N. Haste, S. S. Taylor, A. F. Neuwald, The hallmark of AGC kinase
- 810 functional divergence is its C-terminal tail, a cis-acting regulatory module. *Proc Natl*
- 811 *Acad Sci U S A* **104**, 1272-1277 (2007).
- 812 17. S. S. Taylor, R. Ilouz, P. Zhang, A. P. Kornev, Assembly of allosteric macromolecular
- 813 switches: lessons from PKA. *Nat Rev Mol Cell Biol* **13**, 646-658 (2012).
- 814 18. A. P. Kornev, S. S. Taylor, Dynamics-Driven Allostery in Protein Kinases. *Trends*
- 815 *Biochem Sci* **40**, 628-647 (2015).
- 816 19. M. J. Zoller, S. S. Taylor, Affinity labeling of the nucleotide binding site of the catalytic
- 817 subunit of cAMP-dependent protein kinase using p-fluorosulfonyl-[¹⁴C]benzoyl 5'-

- 818 adenosine. Identification of a modified lysine residue. *J Biol Chem* **254**, 8363-8368
819 (1979).
- 820 20. J. A. Buechler, S. S. Taylor, Dicyclohexylcarbodiimide cross-links two conserved
821 residues, Asp-184 and Lys-72, at the active site of the catalytic subunit of cAMP-
822 dependent protein kinase. *Biochemistry* **28**, 2065-2070 (1989).
- 823 21. B. Nolen, S. Taylor, G. Ghosh, Regulation of protein kinases; controlling activity through
824 activation segment conformation. *Mol Cell* **15**, 661-675 (2004).
- 825 22. L. N. Johnson, M. E. Noble, D. J. Owen, Active and inactive protein kinases: structural
826 basis for regulation. *Cell* **85**, 149-158 (1996).
- 827 23. S. J. Deminoff, S. C. Howard, A. Hester, S. Warner, P. K. Herman, Using substrate-
828 binding variants of the cAMP-dependent protein kinase to identify novel targets and a
829 kinase domain important for substrate interactions in *Saccharomyces cerevisiae*.
830 *Genetics* **173**, 1909-1917 (2006).
- 831 24. S. J. Deminoff, V. Ramachandran, P. K. Herman, Distal recognition sites in substrates
832 are required for efficient phosphorylation by the cAMP-dependent protein kinase.
833 *Genetics* **182**, 529-539 (2009).
- 834 25. H. S. Meharena, P. Chang, M. M. Keshwani, K. Oruganty, A. K. Nene et al., Deciphering
835 the structural basis of eukaryotic protein kinase regulation. *PLoS Biol* **11**, e1001680
836 (2013).
- 837 26. J. Hu, E. C. Stites, H. Yu, E. A. Germino, H. S. Meharena et al., Allosteric activation of
838 functionally asymmetric RAF kinase dimers. *Cell* **154**, 1036-1046 (2013).
- 839 27. A. S. Shaw, A. P. Kornev, J. Hu, L. G. Ahuja, S. S. Taylor, Kinases and pseudokinases:
840 lessons from RAF. *Mol Cell Biol* **34**, 1538-1546 (2014).
- 841 28. D. I. McSkimming, S. Dastgheib, E. Talevich, A. Narayanan, S. Katiyar et al., ProKinO: a
842 unified resource for mining the cancer kinome. *Hum Mutat* **36**, 175-186 (2015).
- 843 29. Z. Ruan, N. Kannan, Altered conformational landscape and dimerization dependency
844 underpins the activation of EGFR by alphaC-beta4 loop insertion mutations. *Proc Natl*
845 *Acad Sci U S A* **115**, E8162-E8171 (2018).
- 846 30. I. Tsigelny, J. P. Greenberg, S. Cox, W. L. Nichols, S. S. Taylor et al., 600 ps molecular
847 dynamics reveals stable substructures and flexible hinge points in cAMP dependent
848 protein kinase. *Biopolymers* **50**, 513-524 (1999).
- 849 31. A. Myasnikov, H. W. Zhu, P. Hixson, B. E. Xie, K. W. Yu et al., Structural analysis of the
850 full-length human LRRK2. *Cell* **184**, 3519+ (2021).
- 851 32. H. Zhu, F. Tonelli, D. R. Alessi, J. Sun, Structural basis of human LRRK2 membrane
852 recruitment and activation. *bioRxiv* **2022.04.26.489605** (2022).
- 853 33. O. Gerlits, K. L. Weiss, M. P. Blakeley, G. Veglia, S. S. Taylor et al., Zooming in on
854 protons: Neutron structure of protein kinase A trapped in a product complex. *Sci Adv* **5**,
855 eaav0482 (2019).
- 856 34. D. C. Wych, P. C. Aoto, L. Vu, A. M. Wolff, D. L. Mobley et al., Molecular-dynamics
857 simulation methods for macromolecular crystallography. *Acta Crystallogr D Struct Biol*
858 **79**, 50-65 (2023).
- 859 35. D. A. Walsh, C. D. Ashby, C. Gonzalez, D. Calkins, E. H. Fischer et al., Purification and
860 characterization of a protein inhibitor of adenosine 3',5'-monophosphate-dependent
861 protein kinases. *J Biol Chem* **246**, 1977-1985 (1971).
- 862 36. C. Olivieri, Y. Wang, G. C. Li, S. M. V, J. Kim et al., Multi-state recognition pathway of
863 the intrinsically disordered protein kinase inhibitor by protein kinase A. *Elife* **9**, e55607
864 (2020).
- 865 37. J. D. Scott, E. H. Fischer, K. Takio, J. G. Demaille, E. G. Krebs, Amino-Acid Sequence
866 of the Heat-Stable Inhibitor of the Camp-Dependent Protein-Kinase from Rabbit
867 Skeletal-Muscle. *P Natl Acad Sci USA* **82**, 5732-5736 (1985).

- 868 38. J. D. Scott, E. H. Fischer, J. G. Demaille, E. G. Krebs, Identification of an Inhibitory
869 Region of the Heat-Stable Protein Inhibitor of the Camp-Dependent Protein-Kinase. *P*
870 *Natl Acad Sci USA* **82**, 4379-4383 (1985).
- 871 39. H. C. Cheng, S. M. van Patten, A. J. Smith, D. A. Walsh, An active twenty-amino-acid-
872 residue peptide derived from the inhibitor protein of the cyclic AMP-dependent protein
873 kinase. *Biochem J* **231**, 655-661 (1985).
- 874 40. S. Whitehouse, D. A. Walsh, Mg X ATP2-dependent interaction of the inhibitor protein of
875 the cAMP-dependent protein kinase with the catalytic subunit. *J Biol Chem* **258**, 3682-
876 3692 (1983).
- 877 41. D. B. Glass, H. C. Cheng, L. Mende-Mueller, J. Reed, D. A. Walsh, Primary structural
878 determinants essential for potent inhibition of cAMP-dependent protein kinase by
879 inhibitory peptides corresponding to the active portion of the heat-stable inhibitor protein.
880 *J Biol Chem* **264**, 8802-8810 (1989).
- 881 42. D. B. Glass, L. J. Lundquist, B. M. Katz, D. A. Walsh, Protein kinase inhibitor-(6-22)-
882 amide peptide analogs with standard and nonstandard amino acid substitutions for
883 phenylalanine 10. Inhibition of cAMP-dependent protein kinase. *J Biol Chem* **264**,
884 14579-14584 (1989).
- 885 43. J. Reed, J. S. De Ropp, J. Trewhella, D. B. Glass, W. K. Liddle et al., Conformational
886 analysis of PKI(5-22)amide, the active inhibitory fragment of the inhibitor protein of the
887 cyclic AMP-dependent protein kinase. *Biochem J* **264**, 371-380 (1989).
- 888 44. F. W. Herberg, S. S. Taylor, Physiological inhibitors of the catalytic subunit of cAMP-
889 dependent protein kinase: effect of MgATP on protein-protein interactions. *Biochemistry*
890 **32**, 14015-14022 (1993).
- 891 45. F. W. Herberg, M. L. Doyle, S. Cox, S. S. Taylor, Dissection of the nucleotide and metal-
892 phosphate binding sites in cAMP-dependent protein kinase. *Biochemistry* **38**, 6352-6360
893 (1999).
- 894 46. C. Kim, N. H. Xuong, S. S. Taylor, Crystal structure of a complex between the catalytic
895 and regulatory (RI α) subunits of PKA. *Science* **307**, 690-696 (2005).
- 896 47. C. Kim, C. Y. Cheng, S. A. Saldanha, S. S. Taylor, PKA-I holoenzyme structure reveals
897 a mechanism for cAMP-dependent activation. *Cell* **130**, 1032-1043 (2007).
- 898 48. L. R. Masterson, L. Shi, E. Metcalfe, J. Gao, S. S. Taylor et al., Dynamically committed,
899 uncommitted, and quenched states encoded in protein kinase A revealed by NMR
900 spectroscopy. *Proc Natl Acad Sci U S A* **108**, 6969-6974 (2011).
- 901 49. C. L. McClendon, A. P. Kornev, M. K. Gilson, S. S. Taylor, Dynamic architecture of a
902 protein kinase. *Proc Natl Acad Sci U S A* **111**, E4623-4631 (2014).
- 903 50. L. G. Ahuja, P. C. Aoto, A. P. Kornev, G. Veglia, S. S. Taylor, Dynamic allostery-based
904 molecular workings of kinase:peptide complexes. *Proc Natl Acad Sci U S A* **116**, 15052-
905 15061 (2019).
- 906 51. M. H. Omar, D. P. Byrne, K. N. Jones, T. M. Lakey, K. B. Collins et al., Mislocalization of
907 protein kinase A drives pathology in Cushing's syndrome. *Cell Rep* **40**, 111073 (2022).
- 908 52. M. H. Omar, M. Kihui, D. P. Byrne, K. S. Lee, T. M. Lakey et al., Classification of
909 Cushing's syndrome PKAc mutants based upon their ability to bind PKI. *Biochem J* **480**,
910 875-890 (2023).
- 911 53. C. Walker, Y. Wang, C. Olivieri, S. M. V, J. Gao et al., Is Disrupted Nucleotide-Substrate
912 Cooperativity a Common Trait for Cushing's Syndrome Driving Mutations of Protein
913 Kinase A? *J Mol Biol* **433**, 167123 (2021).
- 914 54. C. Olivieri, G. C. Li, Y. Wang, S. M. V, C. Walker et al., ATP-competitive inhibitors
915 modulate the substrate binding cooperativity of a kinase by altering its conformational
916 entropy. *Sci Adv* **8**, eabo0696 (2022).

- 917 55. C. Walker, Y. Wang, C. Olivieri, A. Karamafrooz, J. Casby et al., Cushing's syndrome
918 driver mutation disrupts protein kinase A allosteric network, altering both regulation and
919 substrate specificity. *Sci Adv* **5**, eaaw9298 (2019).
- 920 56. J. Wu, J. Yang, N. Kannan, Madhusudan, N. H. Xuong et al., Crystal structure of the
921 E230Q mutant of cAMP-dependent protein kinase reveals an unexpected apoenzyme
922 conformation and an extended N-terminal A helix. *Protein Sci* **14**, 2871-2879 (2005).
- 923 57. L. G. Ahuja, A. P. Kornev, C. L. McClendon, G. Veglia, S. S. Taylor, Mutation of a kinase
924 allosteric node uncouples dynamics linked to phosphotransfer. *Proc Natl Acad Sci U S A*
925 **114**, E931-E940 (2017).
- 926 58. L. G. Ahuja, S. S. Taylor, A. P. Kornev, Tuning the "violin" of protein kinases: The role of
927 dynamics-based allostery. *IUBMB Life* **71**, 685-696 (2019).
- 928 59. L. K. Madan, C. L. Welsh, A. P. Kornev, S. S. Taylor, The "violin model": Looking at
929 community networks for dynamic allostery. *J Chem Phys* **158**, 081001 (2023).
- 930 60. E. J. Kennedy, J. Yang, L. Pillus, S. S. Taylor, G. Ghosh, Identifying critical non-catalytic
931 residues that modulate protein kinase A activity. *PLoS One* **4**, e4746 (2009).
- 932 61. R. M. Gibson, S. S. Taylor, Dissecting the cooperative reassociation of the regulatory
933 and catalytic subunits of cAMP-dependent protein kinase. Role of Trp-196 in the
934 catalytic subunit. *J Biol Chem* **272**, 31998-32005 (1997).
- 935 62. C. Olivieri, Y. Wang, C. Walker, M. V. Subrahmanian, K. N. Ha et al., The aC-b4 loop
936 controls the allosteric cooperativity between nucleotide and substrate in the catalytic
937 subunit of protein kinase A. *eLife*, submitted (2023).
- 938 63. T. Pawson, J. D. Scott, Signaling through scaffold, anchoring, and adaptor proteins.
939 *Science* **278**, 2075-2080 (1997).
- 940 64. G. A. Huber, J. A. McCammon, Brownian Dynamics Simulations of Biological Molecules.
941 *Trends Chem* **1**, 727-738 (2019).
- 942 65. S. H. Northrup, S. A. Allison, J. A. Mccammon, Brownian Dynamics Simulation of
943 Diffusion-Influenced Bimolecular Reactions. *Journal of Chemical Physics* **80**, 1517-1526
944 (1984).
- 945 66. P. I. Poulidakos, C. Zhang, G. Bollag, K. M. Shokat, N. Rosen, RAF inhibitors
946 transactivate RAF dimers and ERK signalling in cells with wild-type BRAF. *Nature* **464**,
947 427-430 (2010).
- 948 67. A. L. Garske, U. Peters, A. T. Cortesi, J. L. Perez, K. M. Shokat, Chemical genetic
949 strategy for targeting protein kinases based on covalent complementarity. *Proc Natl*
950 *Acad Sci U S A* **108**, 15046-15052 (2011).
- 951 68. A. P. Kornev, P. C. Aoto, S. S. Taylor, Calculation of centralities in protein kinase A.
952 *Proc Natl Acad Sci U S A* **119**, e2215420119 (2022).
- 953 69. A. Cooper, D. T. Dryden, Allostery without conformational change. A plausible model.
954 *Eur Biophys J* **11**, 103-109 (1984).
- 955 70. N. Popovych, S. Sun, R. H. Ebright, C. G. Kalodimos, Dynamically driven protein
956 allostery. *Nat Struct Mol Biol* **13**, 831-838 (2006).
- 957 71. C. M. Petit, J. Zhang, P. J. Sapienza, E. J. Fuentes, A. L. Lee, Hidden dynamic allostery
958 in a PDZ domain. *Proc Natl Acad Sci U S A* **106**, 18249-18254 (2009).
- 959 72. L. Di Paola, A. Giuliani, Protein contact network topology: a natural language for
960 allostery. *Curr Opin Struct Biol* **31**, 43-48 (2015).
- 961 73. M. Jacomy, T. Venturini, S. Heymann, M. Bastian, ForceAtlas2, a continuous graph
962 layout algorithm for handy network visualization designed for the Gephi software. *PLoS*
963 *One* **9**, e98679 (2014).
- 964 74. D. A. Case, T. E. Cheatham, 3rd, T. Darden, H. Gohlke, R. Luo et al., The Amber
965 biomolecular simulation programs. *J Comput Chem* **26**, 1668-1688 (2005).

- 966 75. P. Akamine, Madhusudan, J. Wu, N. H. Xuong, L. F. Ten Eyck et al., Dynamic features
967 of cAMP-dependent protein kinase revealed by apoenzyme crystal structure. *J Mol Biol*
968 **327**, 159-171 (2003).
- 969 76. J. A. Maier, C. Martinez, K. Kasavajhala, L. Wickstrom, K. E. Hauser et al., ff14SB:
970 Improving the Accuracy of Protein Side Chain and Backbone Parameters from ff99SB. *J*
971 *Chem Theory Comput* **11**, 3696-3713 (2015).
- 972 77. M. H. M. Olsson, C. R. Søndergaard, M. Rostkowski, J. H. Jensen. PROPKA3:
973 Consistent
974 Treatment of Internal and Surface Residues in Empirical $p K_a$ Predictions. *Journal of*
975 *Chemical Theory and Computation*, **7**, 525–537 (2011).
- 976 78. C. R. Søndergaard, M. H. M. Olsson, M. Rostkowski, J. H. Jensen, Improved Treatment
977 of Ligands and Coupling Effects in Empirical Calculation and Rationalization of $p K_a$
978 Values. *Journal of Chemical Theory and Computation*, **7**, 2284–2295 (2011).
- 979 79. K. L. Meagher, L. T. Redman, H. A. Carlson. Development of polyphosphate parameters
980 for use with the AMBER force field. *Journal of Computational Chemistry*, **24**, 1016–1025
981 (2003).
- 982 80. O. Allnér, L. Nilsson, A. Villa. Magnesium Ion–Water Coordination and Exchange in
983 Biomolecular Simulations. *Journal of Chemical Theory and Computation*, **8**, 1493–1502
984 (2012).
- 985 81. N. Homeyer, A. H. Horn, H. Lanig, H. Sticht, AMBER force-field parameters for
986 phosphorylated amino acids in different protonation states: phosphoserine,
987 phosphothreonine, phosphotyrosine, and phosphohistidine. *J Mol Model* **12**, 281-289
988 (2006).
- 989 82. D. J. Price, C. L. Brooks, 3rd, A modified TIP3P water potential for simulation with Ewald
990 summation. *J Chem Phys* **121**, 10096-10103 (2004).
- 991 83. R. J. Loncharich, B. R. Brooks, R. W. Pastor, Langevin dynamics of peptides: the
992 frictional dependence of isomerization rates of N-acetylalanyl-N'-methylamide.
993 *Biopolymers* **32**, 523-535 (1992).
- 994 84. R. W. Pastor, B. R. Brooks, A. Szabo, An Analysis of the Accuracy of Langevin and
995 Molecular-Dynamics Algorithms. *Mol Phys* **65**, 1409-1419 (1988).
- 996 85. H. J. C. Berendsen, J. P. M. Postma, W. F. Vangunsteren, A. Dinola, J. R. Haak,
997 Molecular-Dynamics with Coupling to an External Bath. *Journal of Chemical Physics* **81**,
998 3684-3690 (1984).
- 999 86. T. Darden, D. York, L. Pedersen, Particle Mesh Ewald - an N.Log(N) Method for Ewald
1000 Sums in Large Systems. *Journal of Chemical Physics* **98**, 10089-10092 (1993).
- 1001 87. M. A. Balsera, W. Wriggers, Y. Oono, K. Schulten, Principal component analysis and
1002 long time protein dynamics. *J Phys Chem-US* **100**, 2567-2572 (1996).
- 1003 88. I. Bahar, A. R. Atilgan, M. C. Demirel, B. Erman, Vibrational dynamics of folded proteins:
1004 Significance of slow and fast motions in relation to function and stability. *Physical*
1005 *Review Letters* **80**, 2733-2736 (1998).
- 1006 89. G. G. Maisuradze, A. Liwo, H. A. Scheraga, Principal component analysis for protein
1007 folding dynamics. *J Mol Biol* **385**, 312-329 (2009).
- 1008 90. H. Frauenfelder, S. G. Sligar, P. G. Wolynes, The Energy Landscapes and Motions of
1009 Proteins. *Science* **254**, 1598-1603 (1991).
- 1010 91. G. G. Maisuradze, A. Liwo, H. A. Scheraga, Relation between Free Energy Landscapes
1011 of Proteins and Dynamics. *Journal of Chemical Theory and Computation* **6**, 583-595
1012 (2010).
- 1013



C

	220	230
PKA	KAVD W WALGVLIYEMAA	
BRAF	FQSD V YAFGIVLYELMT	
LRRK2	QQAD V YSFGLLLYDILT	
PKC β	KSV D W W AFGVLLYEMLA	
PKC α	KSV D W W AYGVLLYEMLA	
SRC	IKSD V W S FGILLT E LTT	

Figure 1

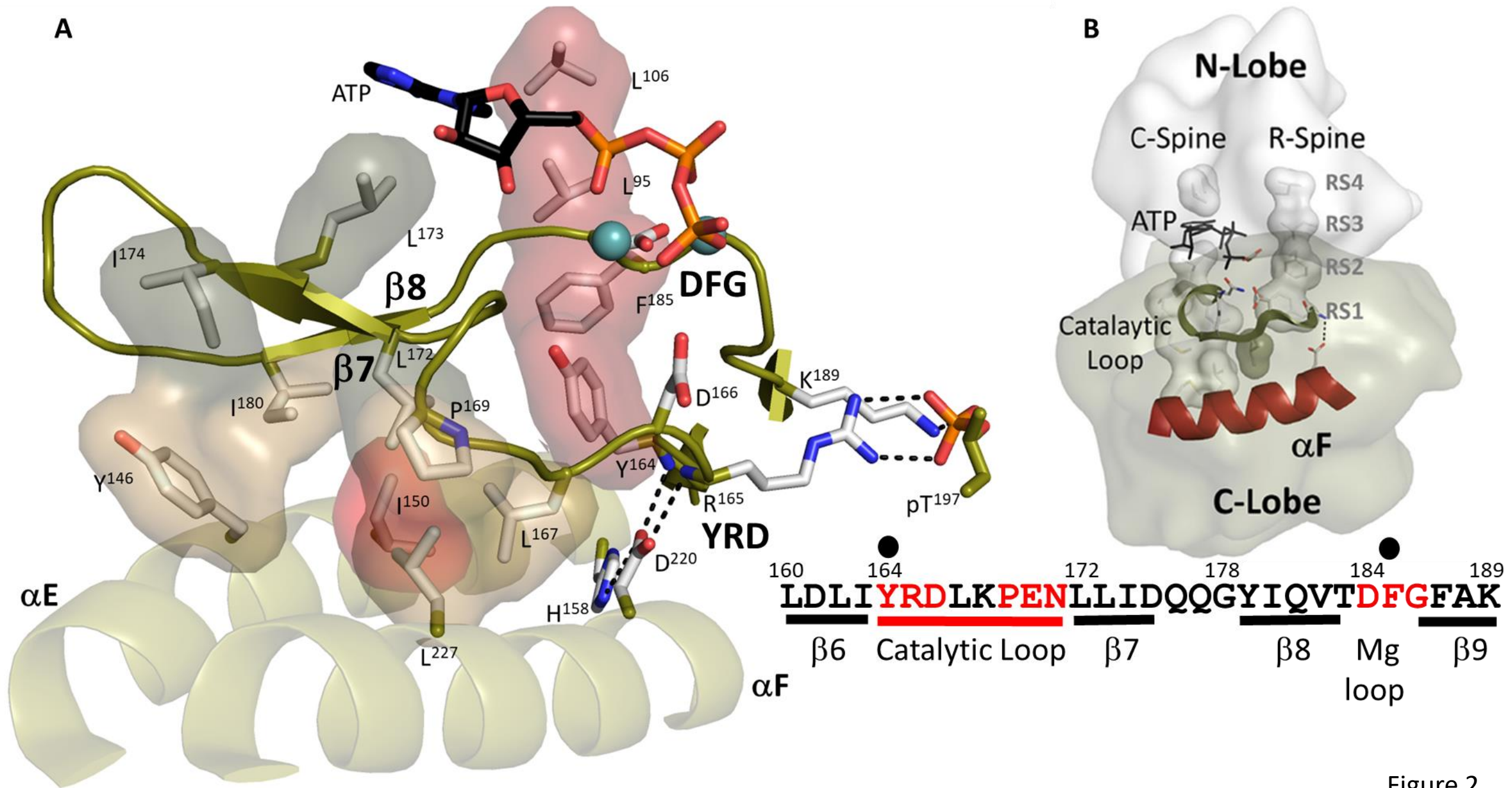


Figure 2

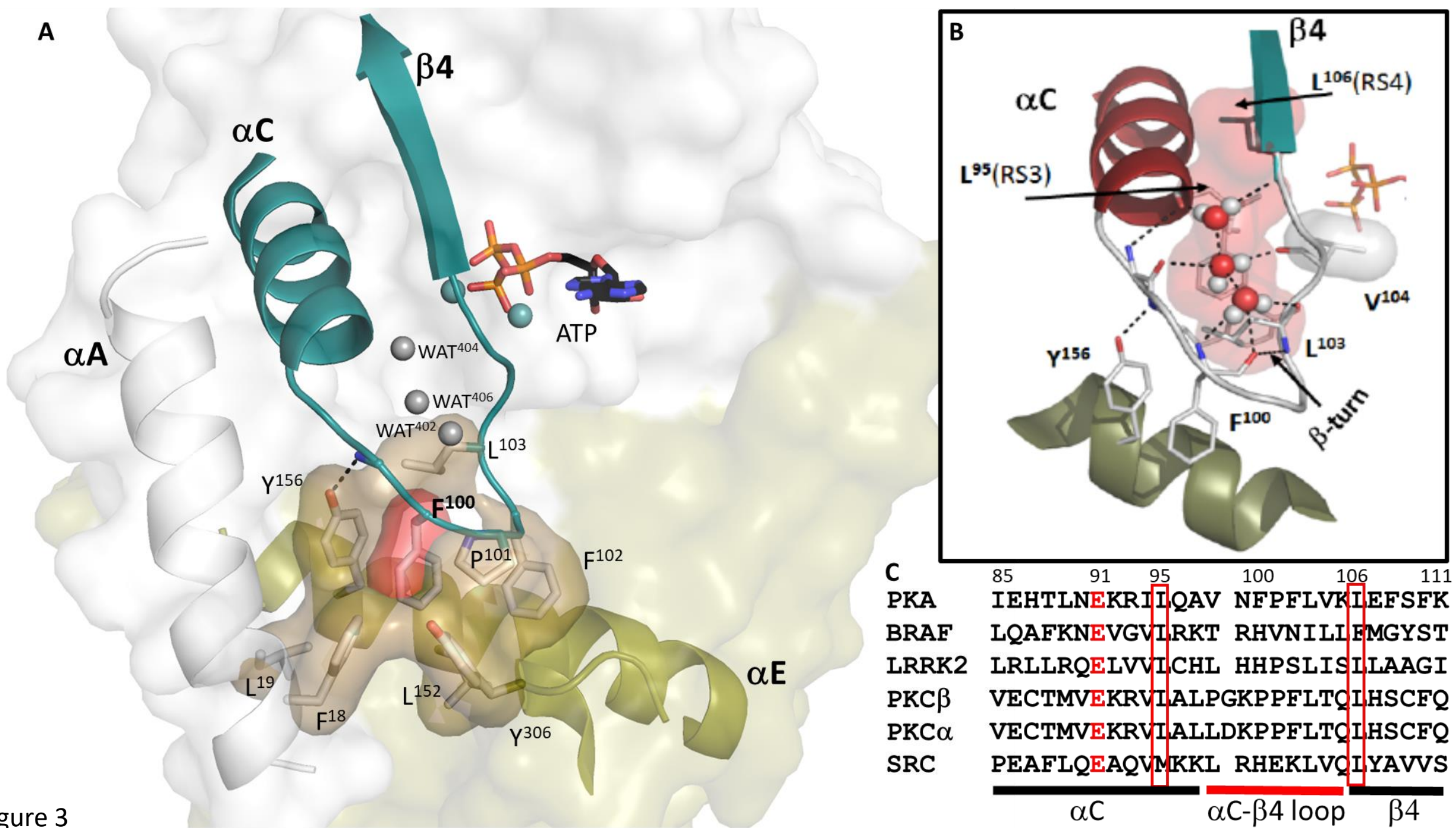
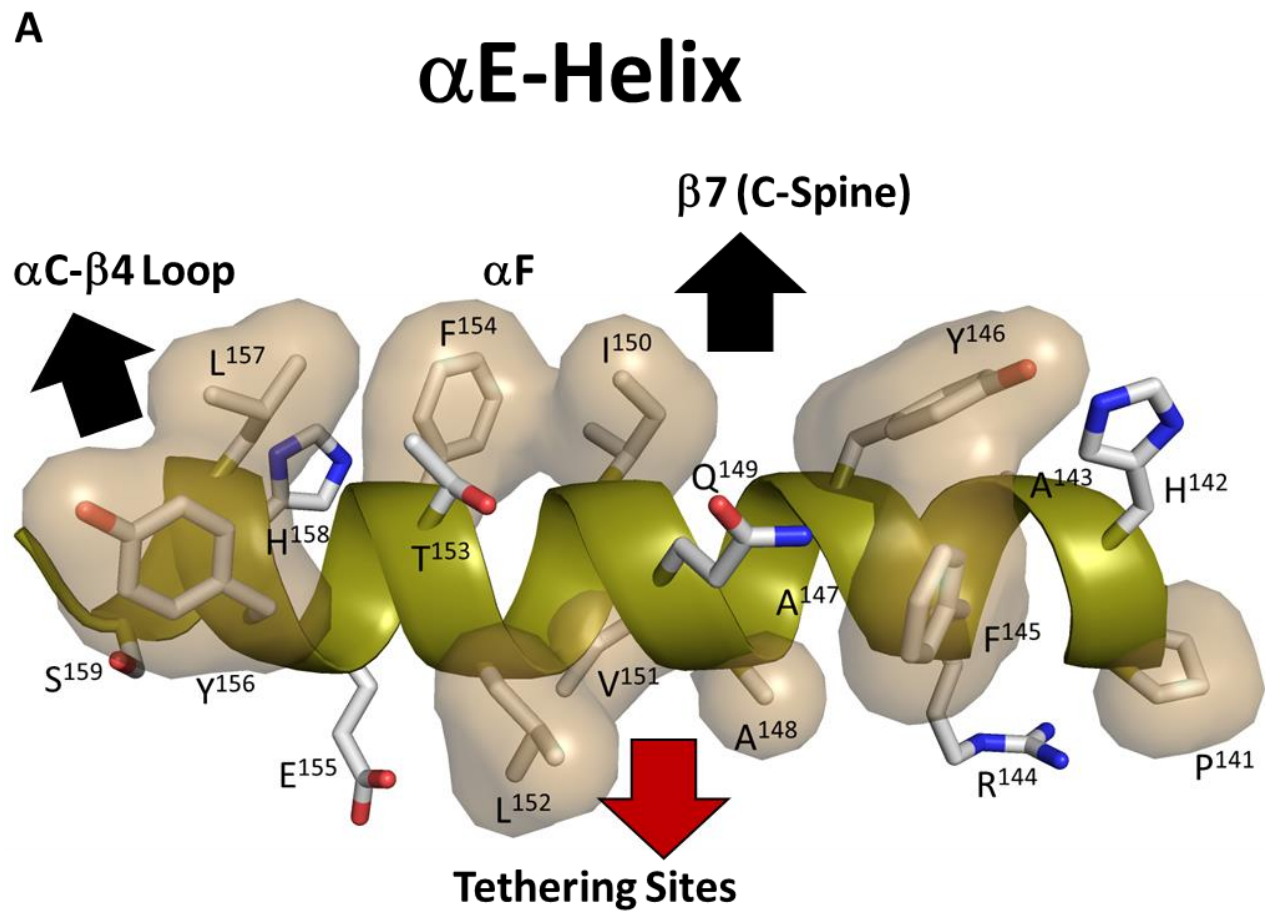


Figure 3



C

	140	146	156	160
PKA	EPHAREYAAQIVLTFEYLHSL			
BRAF	MIKLIDTARQTAQGMDYLHAK			
LRRK2	RTLQHRIALHVADGLRYLHSA			
PKC β	EPHAEVYAAEIAIGLFFLQSK			
PKC α	EPQAVEYAAEISIGLFFLHKR			
SRC	LPQLVDMAAQIASGMAYVERM			

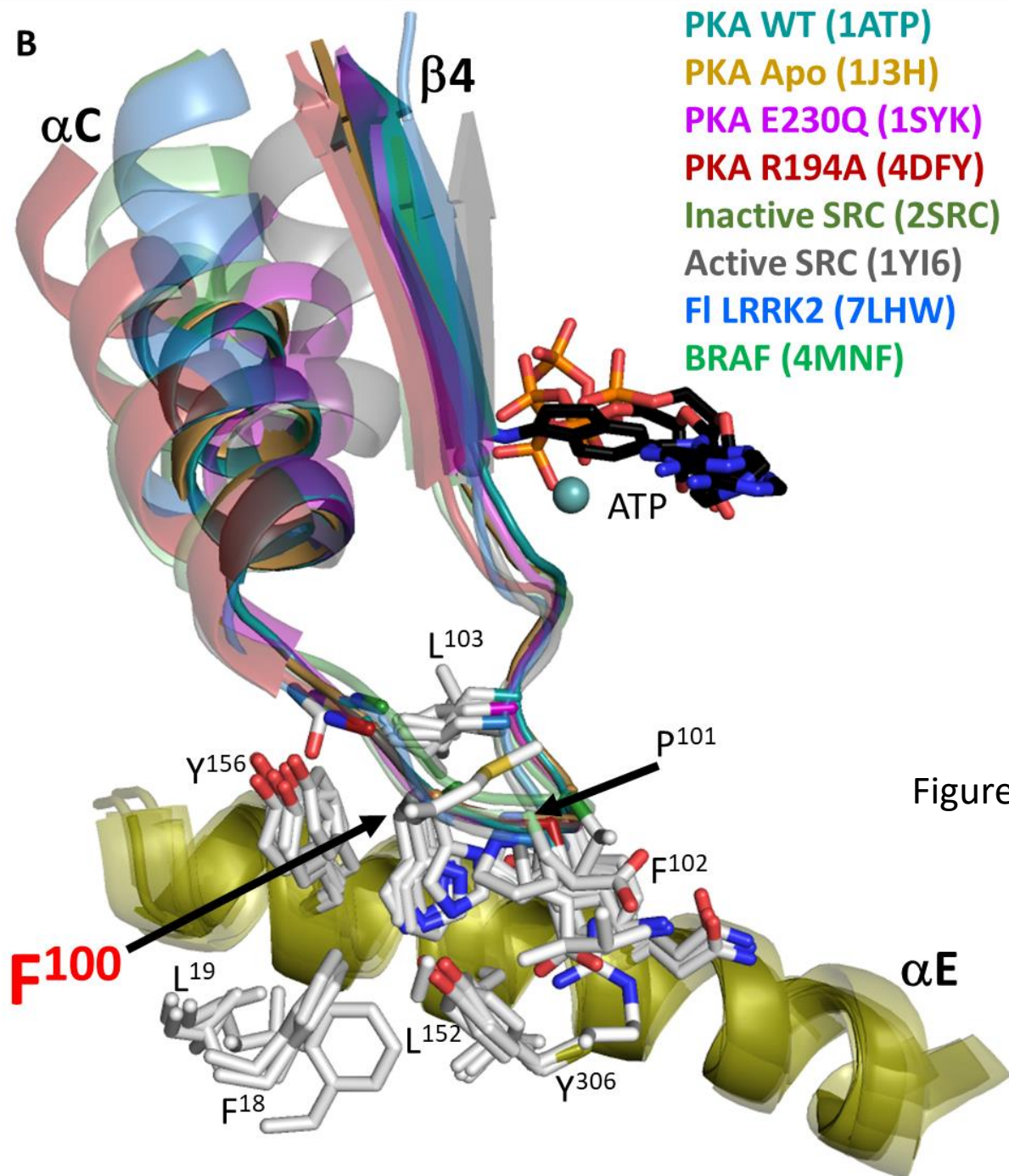


Figure 4

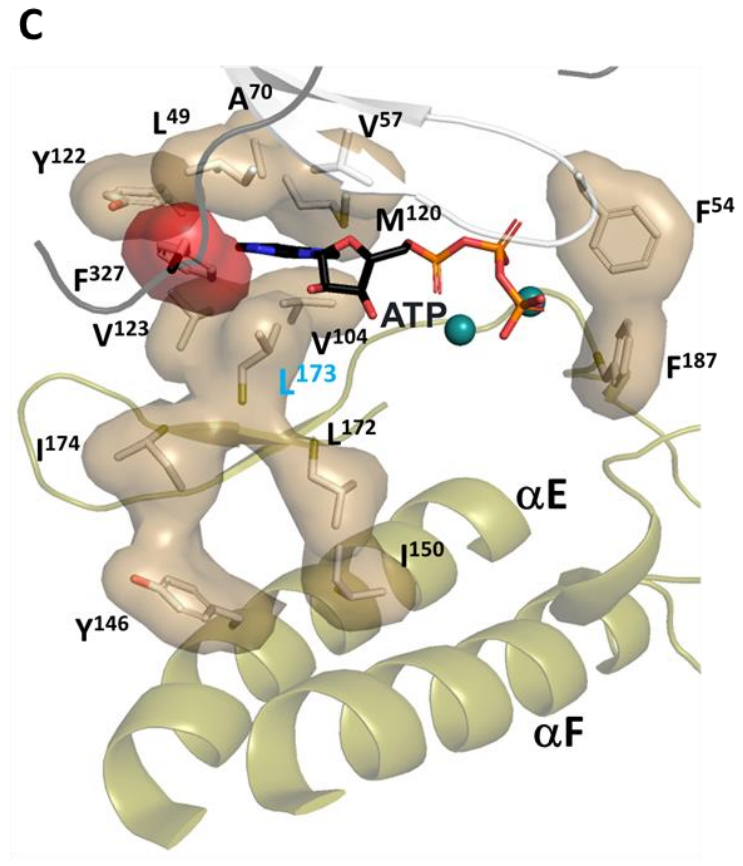
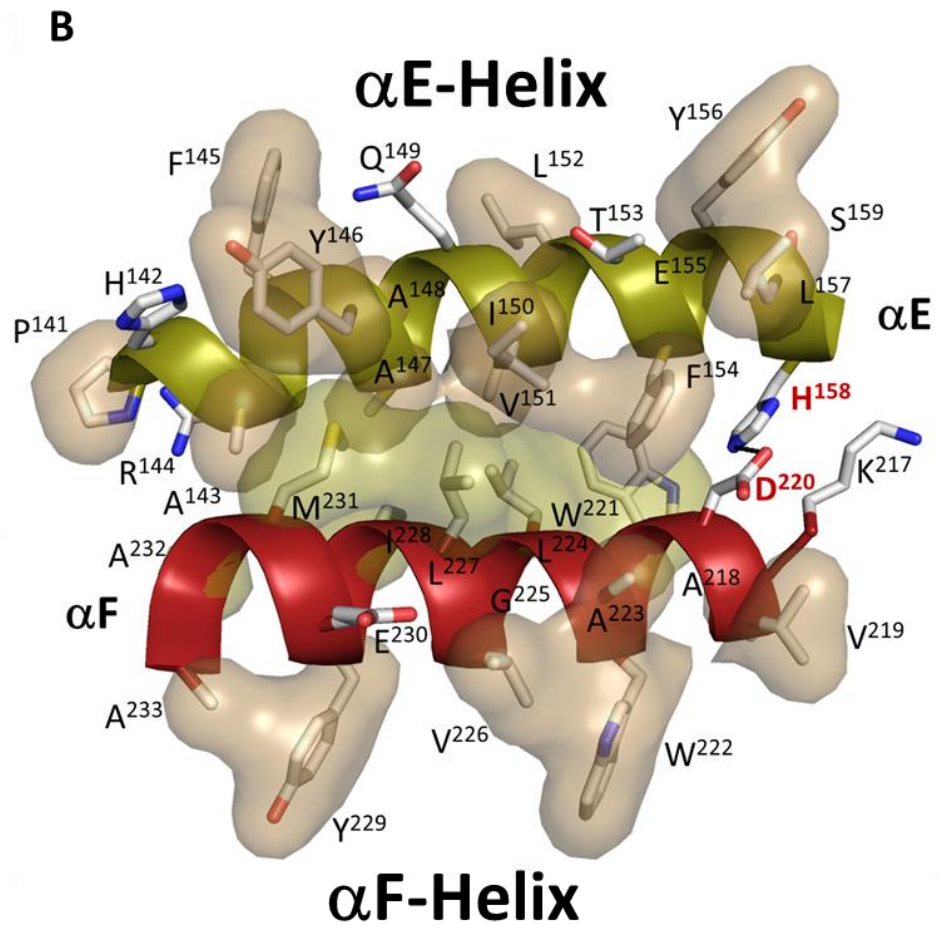
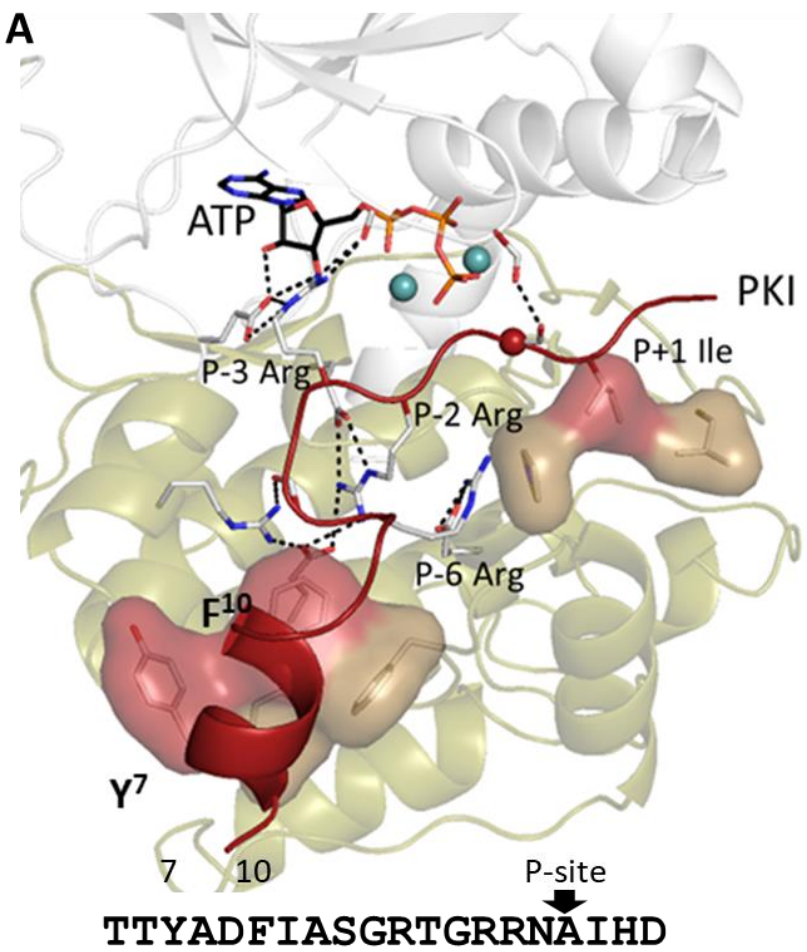


Figure 5

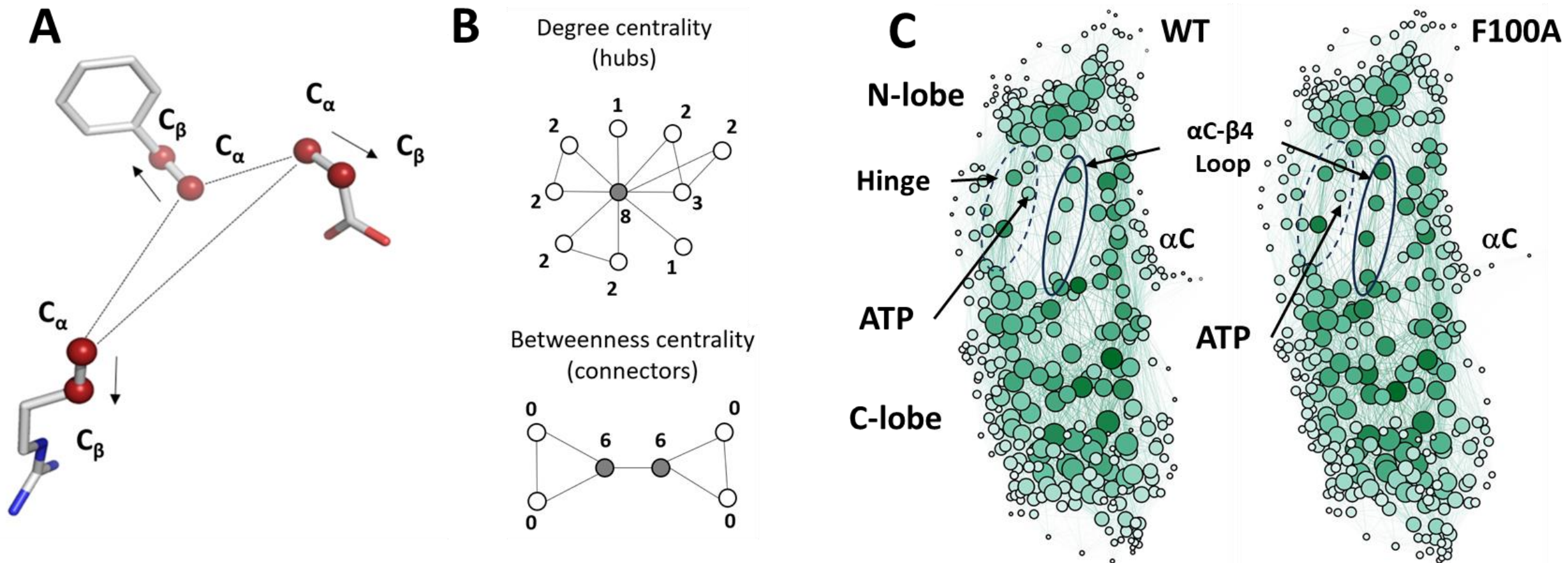


Figure 6

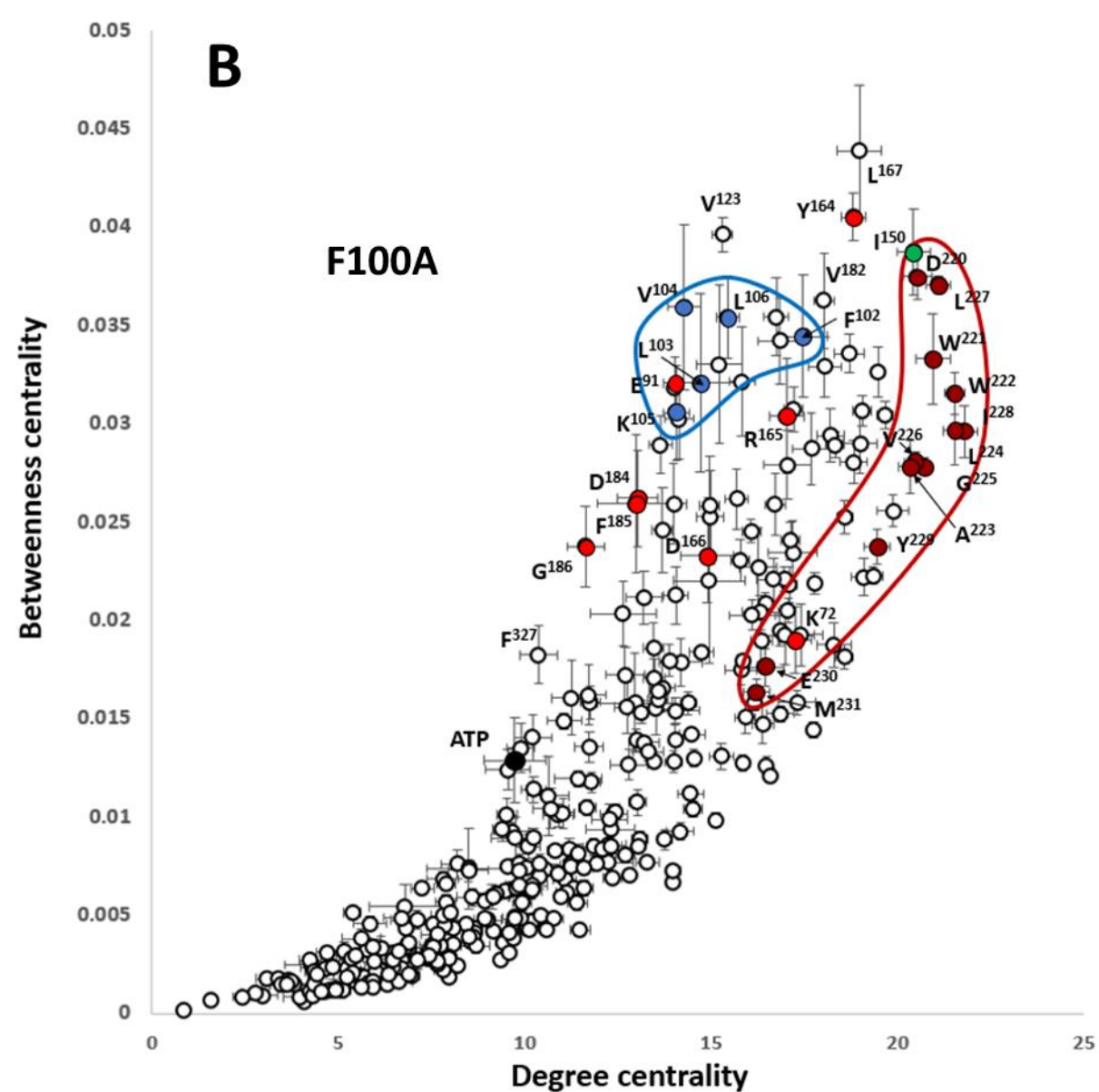
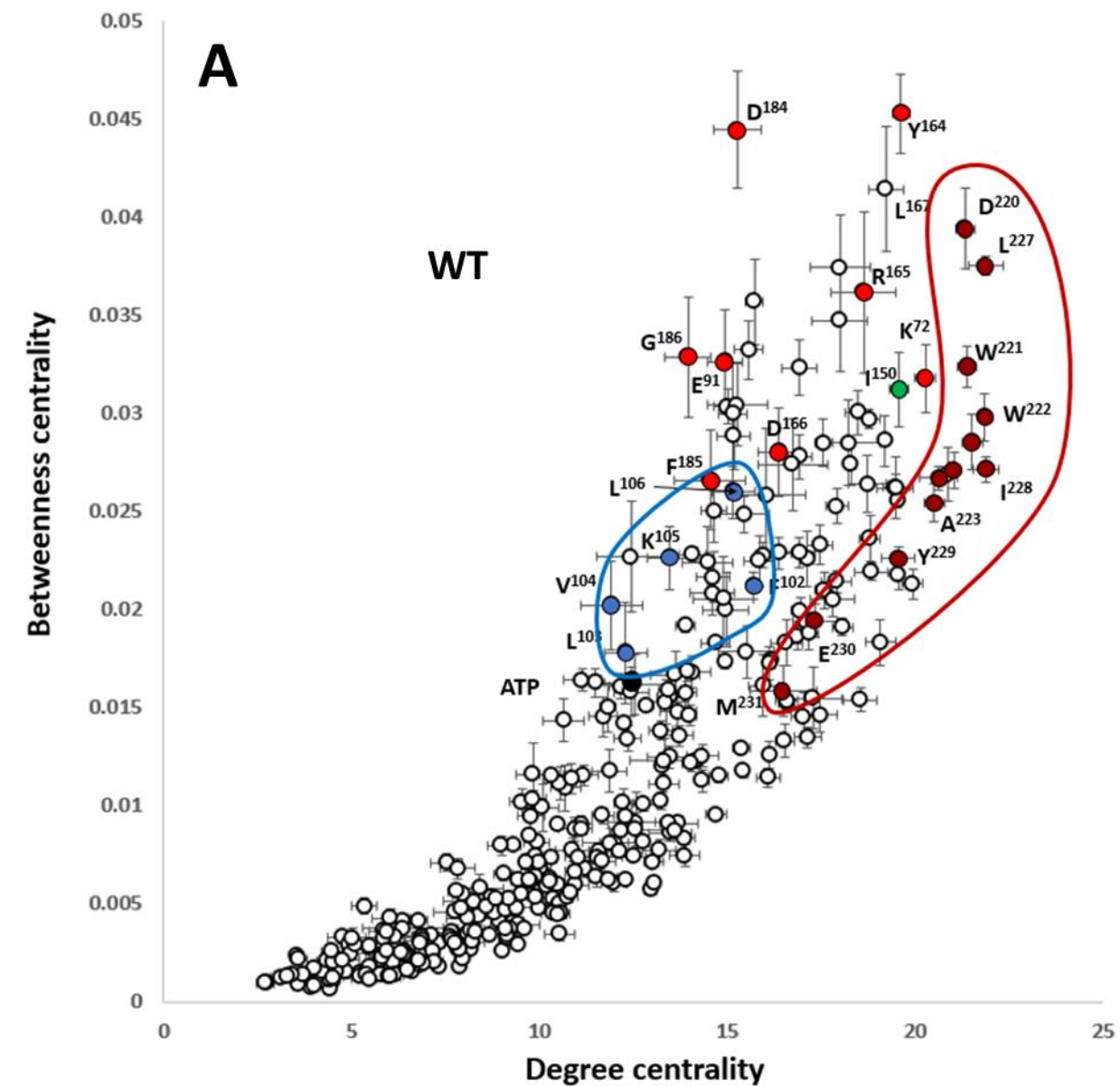


Figure 7

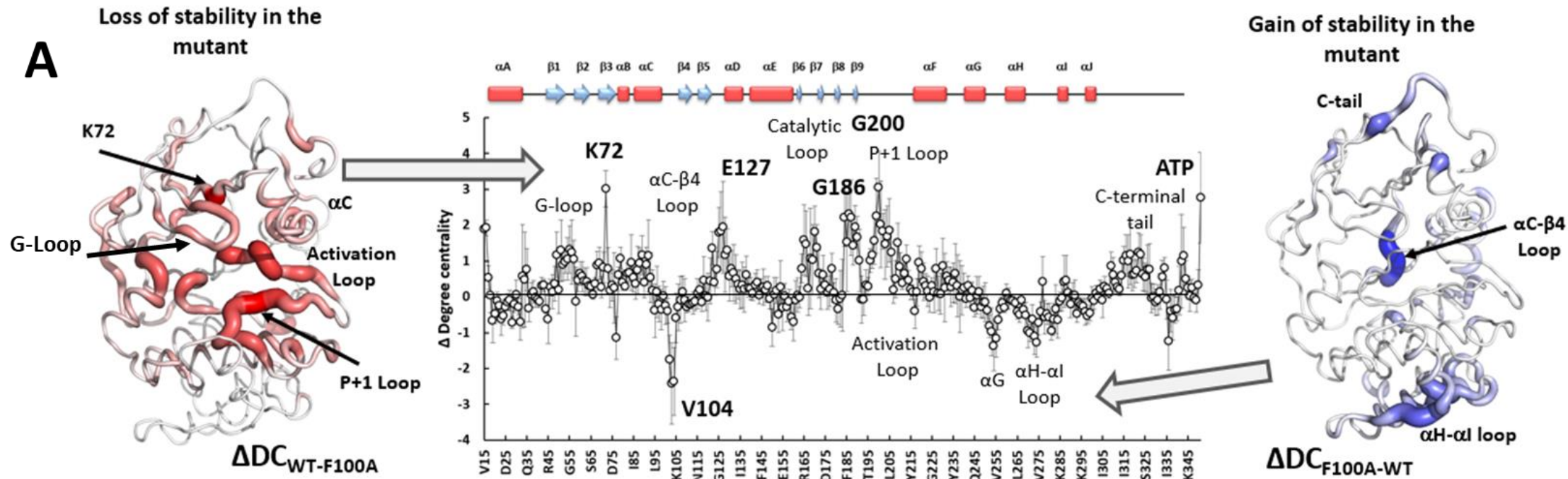


Figure 8

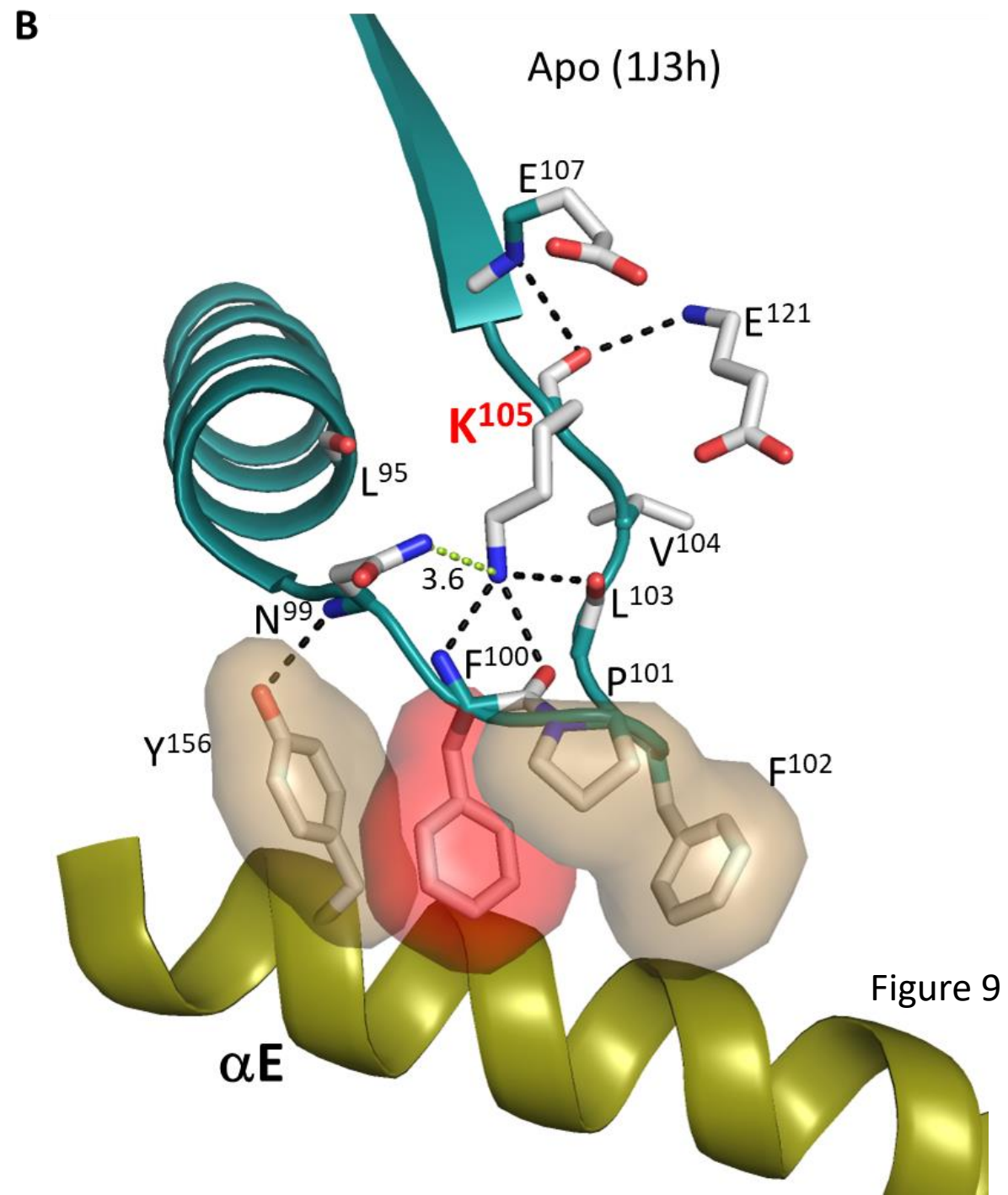
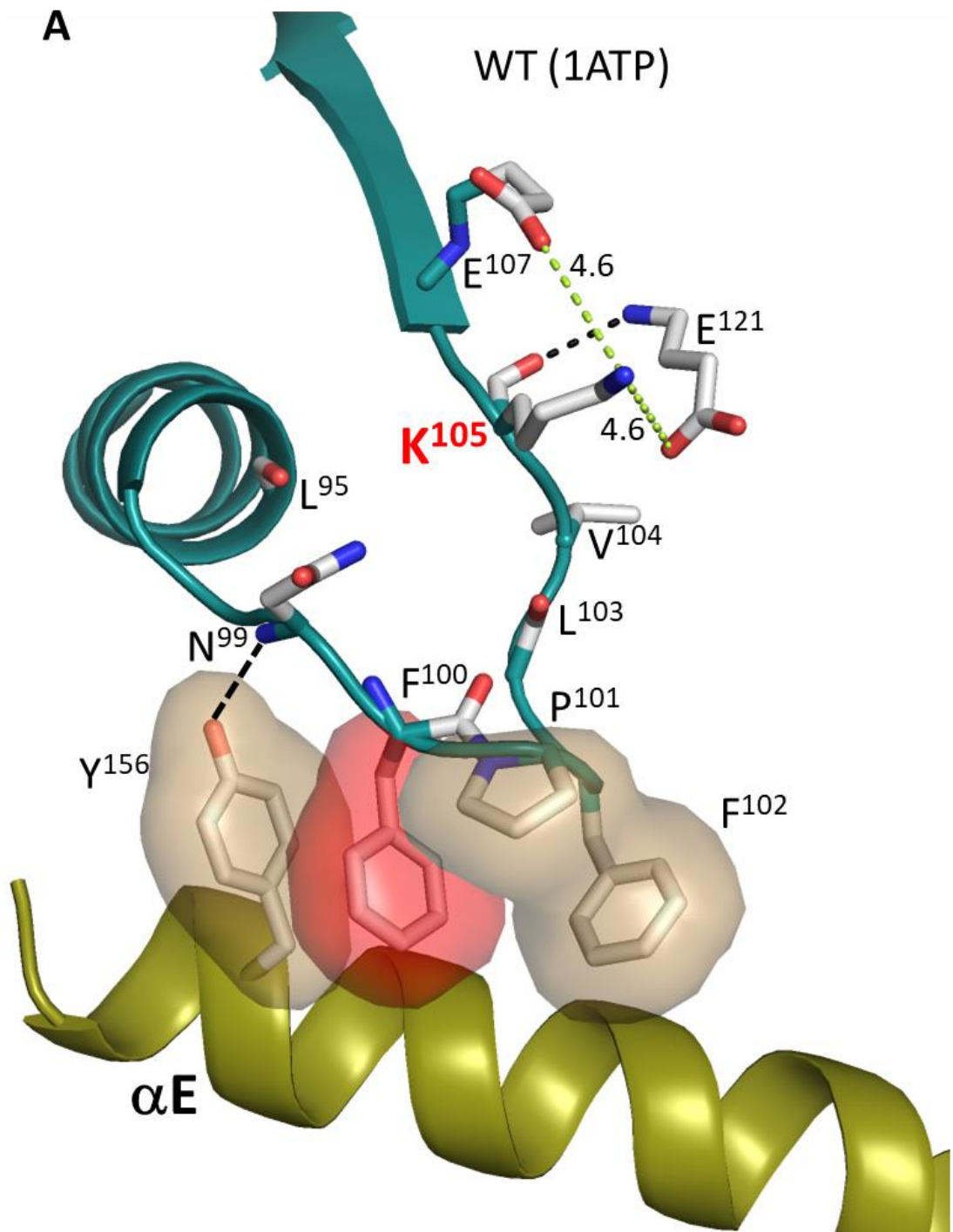


Figure 9

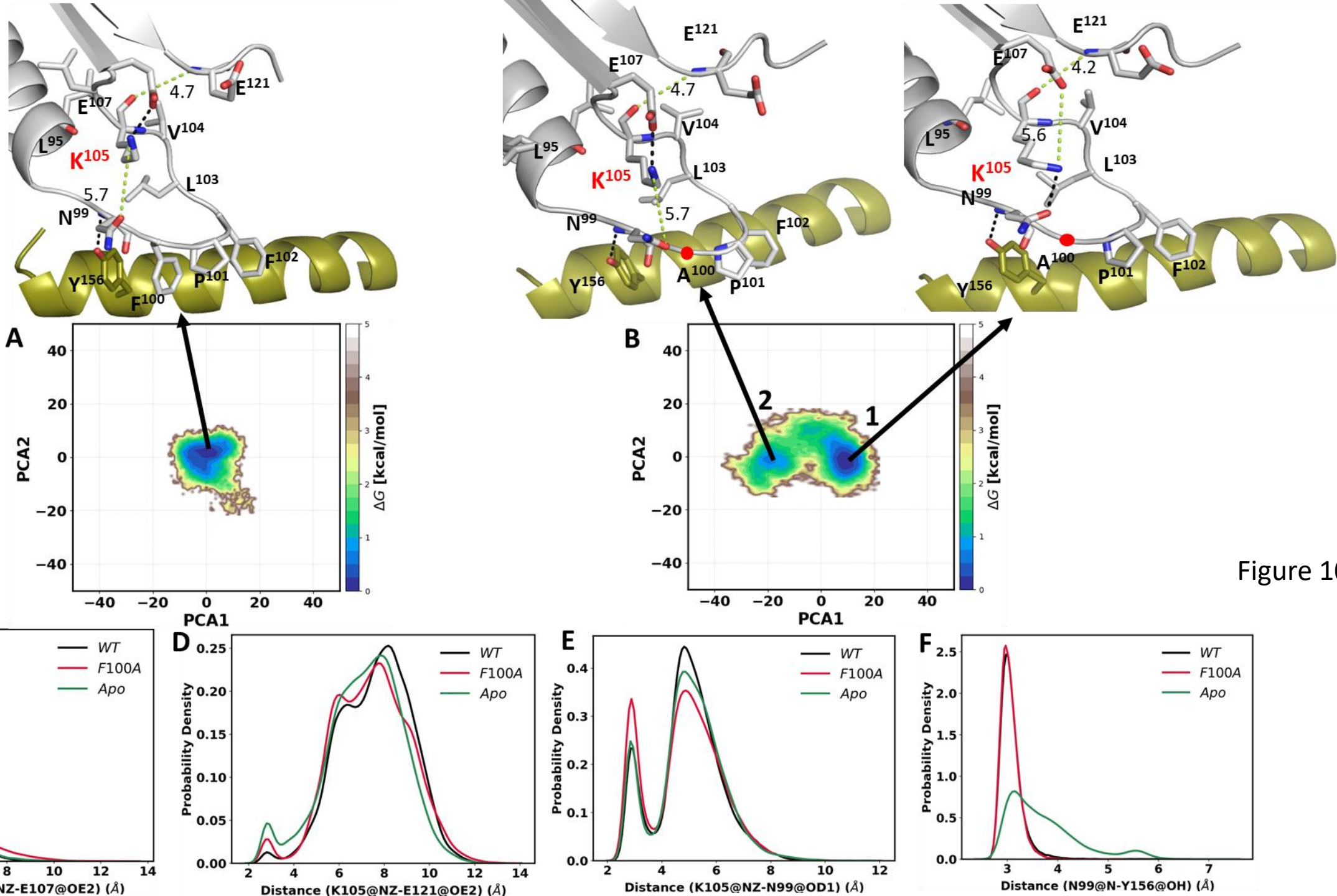
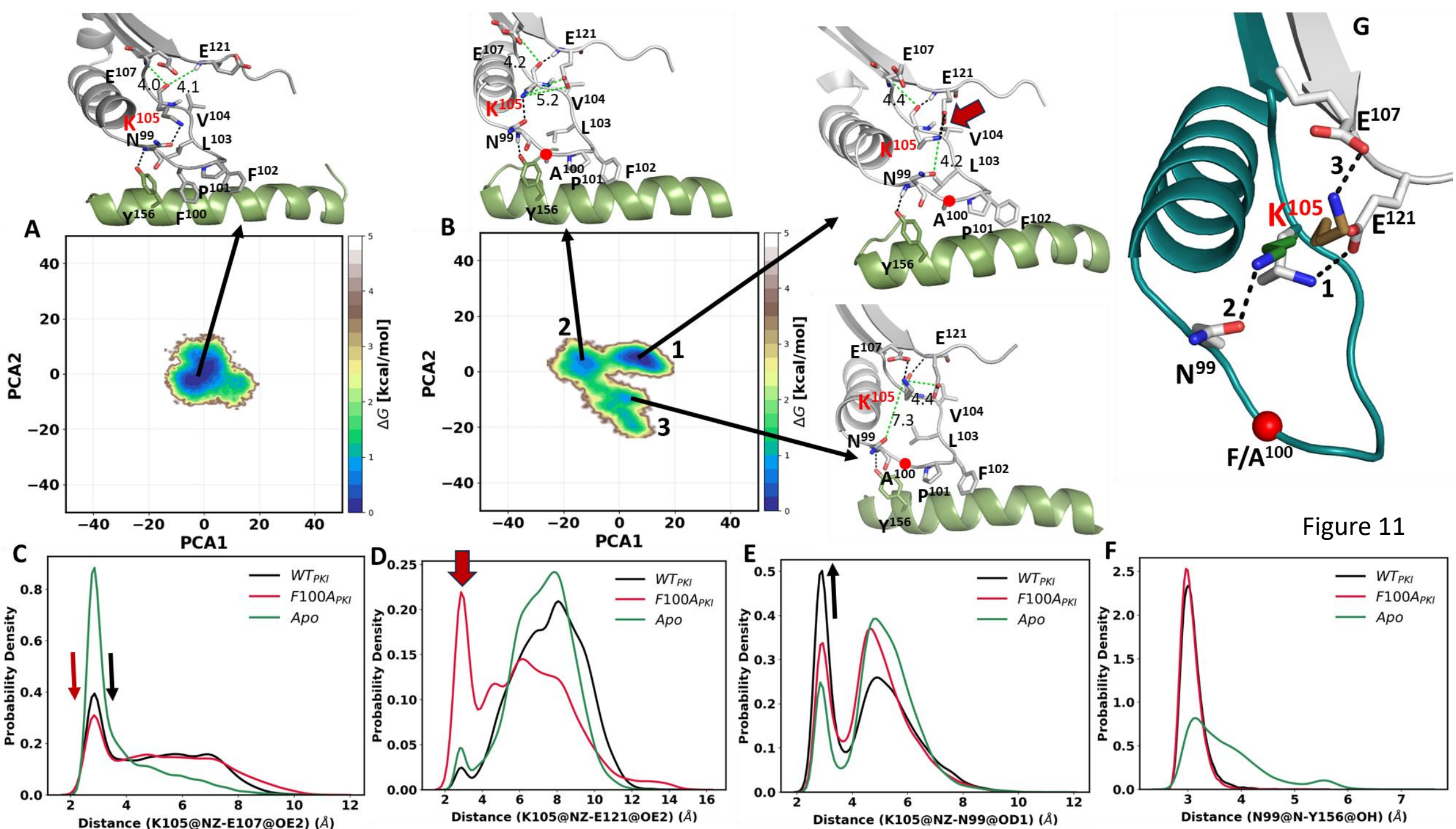


Figure 10



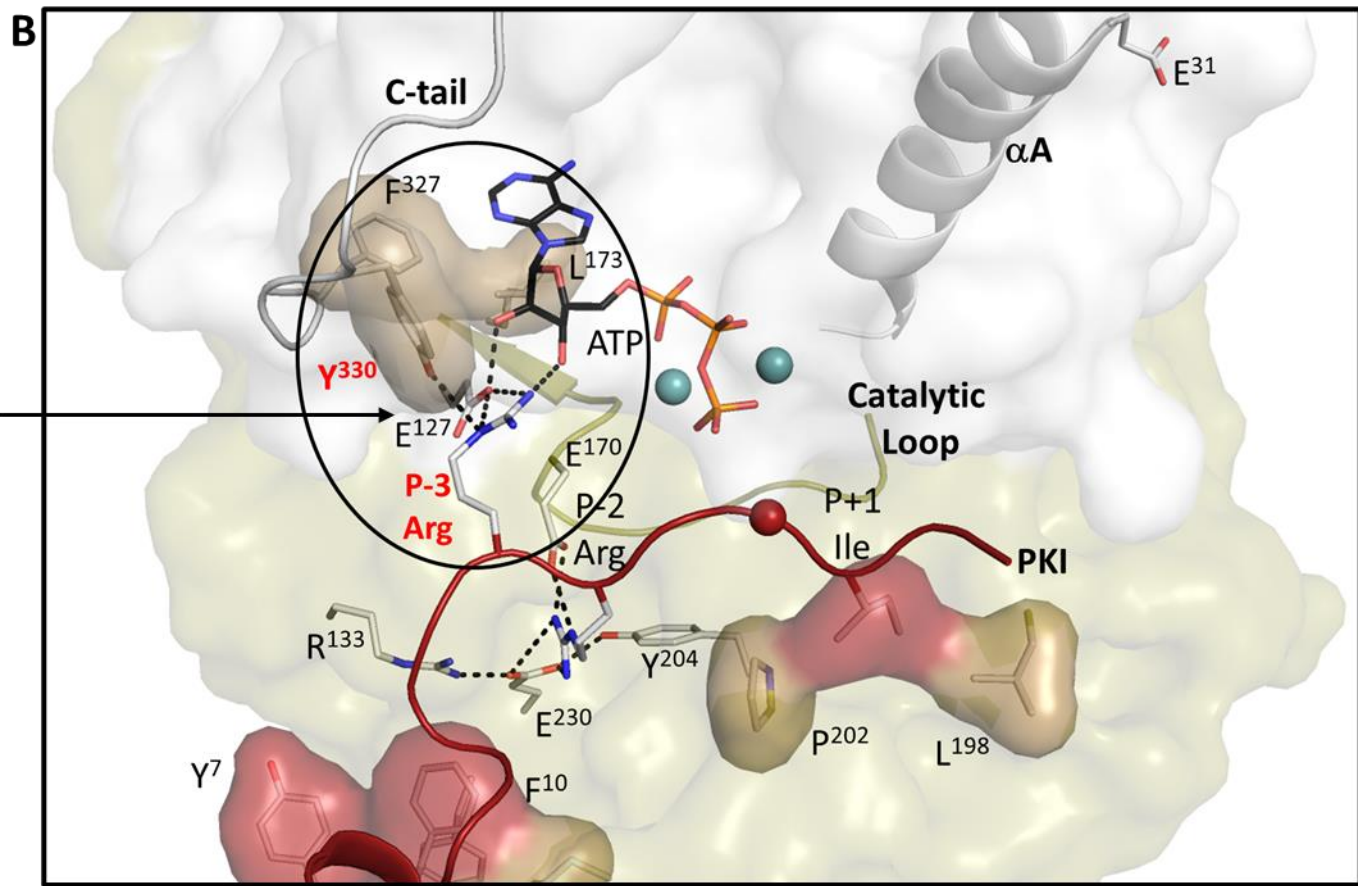
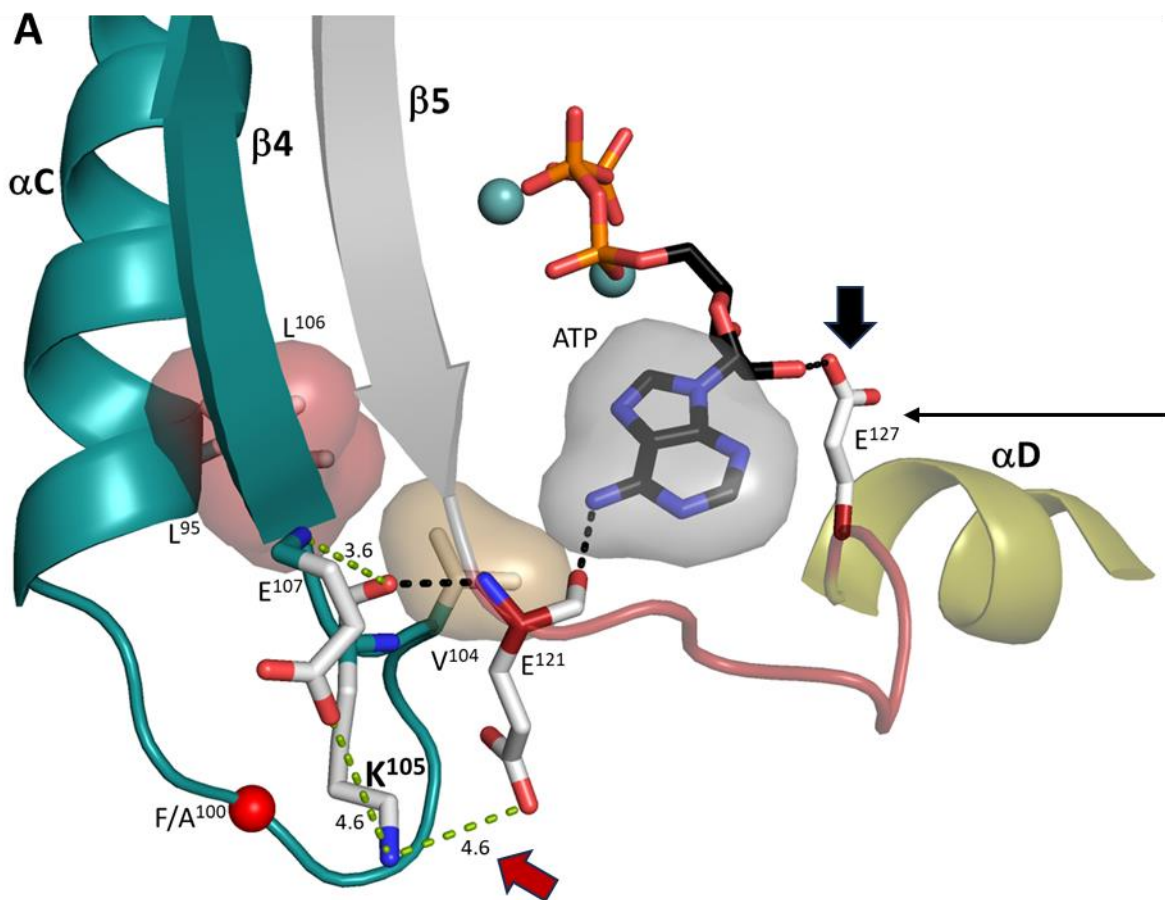


Figure 12